University of Alberta
Printing Department

Digitized by the Internet Archive
in 2019 with funding from
University of Alberta Libraries

https://archive.org/details/Sadiq1965

Thesis
1965
H72

THE UNIVERSITY OF ALBERTA

THE INERTIAL RESISTANCE COEFFICIENT AND OTHER RESERVOIR ROCK PROPERTIES

by

S. Sadiq

A THESIS

SUBMITTED TO THE FACULTY OF GRADUATE STUDIES

IN PARTIAL FULFILLMENT OF THE REQUIREMENTS FOR THE

DEGREE OF MASTER OF SCIENCE

IN

PETROLEUM ENGINEERING

FACULTY OF ENGINEERING

DEPARTMENT OF CHEMICAL AND PETROLEUM ENGINEERING

EDMONTON, ALBERTA

JANUARY, 1965

UNIVERSITY OF ALBERTA

FACULTY OF GRADUATE STUDIES

The undersigned certify that they have read, and recommend to the Faculty of Graduate Studies for acceptance a thesis entitled

THE INERTIAL RESISTANCE COEFFICIENT AND

OTHER RESERVOIR ROCK PROPERTIES

submitted by S. Sadiq, B.E. (Electrical and Mechanical), D.I.C. in partial fulfillment for the degree of Master of Science in Petroleum Engineering.

ABSTRACT

A correlation has been developed between the inertial resistance coefficient and reservoir rock properties such as porosity, permeability and formation resistivity factor. Unlike other correlations, this is dimensionally consistent and does not assume the Kozeny model for porous media.

Experimental determinations on twenty reservoir rock samples have shown interrelationships among the inertial resistance coefficient, porosity, permeability, formation resistivity factor and tortuosity. Data on porosity and formation resistivity factor indicates that their product equals approximately four. This is in agreement with other published data.

A method has been devised to ensure passage of electric current through brine saturated rock samples with fractured ends, without developing contact resistances at the current electrodes.

Permeability data have indicated that the Klinkenberg permeability values may be 100% to 200% in error if proper care is not exercised to limit the flow rate to the viscous flow region.

ACKNOWLEDGEMENTS

The author is indebted to:

Professor P.M. Dranchuk, Department of Chemical and Petroleum Engineering, University of Alberta, who suggested the problem and gave valuable advice during its investigation.

Dr. D.L. Flock of the same Department for reviewing the interpretation of results.

The National Research Council and the Alberta Research Council for making this work possible by granting a Graduate Assistantship in Petroleum Engineering.

Mr. J.D. Clark of the Chemical and Geological Laboratories Limited, Edmonton, for supplying the reservoir rock samples and allowing use of the permeability equipment.

Messrs. Robert Mackett and Marco Leal, graduate students of the Department for many helpful suggestions and discussions.

His parents and his wife whose encouragement became a part of the incentive to complete this project.

TABLE OF CONTENTS

	Page
LIST OF TABLES	i
LIST OF FIGURES	iii
INTRODUCTION	1
THEORY	4
EXPERIMENTAL EQUIPMENT	12
EXPERIMENTAL PROCEDURE	20
Sample Preparation	20
Porosity Measurement	21
Permeability Measurement	21
Electrical Resistance Measurement	25
DISCUSSION OF EXPERIMENTAL RESULTS	27
CONCLUSIONS AND RECOMMENDATIONS	49
NOMENCLATURE	51
BIBLIOGRAPHY	53
APPENDIX I	56
APPENDIX II	78-A
APPENDIX III	[illegible]

LIST OF TABLES

Table Number	Title	Page
1	Physical Properties and Porosity Data	22
2	Summary of Porosity, Permeability and Inertial Resistance Coefficient Data	33
3	Formation Resistivity Factor and Tortuosity Data	47
4	Brine Saturation Data	57
5	Viscous Flow Data - Core No. 4X	58
6	Visco-Inertial Data - Core No. 4X	59
7	Viscous Flow Data - Core No. 20	60
8	Visco-Inertial Data - Core No. 20	61
9	Viscous Flow Data - Core No. 22	62
10	Visco-Inertial Data - Core No. 22	63
11	Viscous Flow Data - Core No. 24	64
12	Visco-Inertial Flow Data - Core No. 24	65
13	Viscous Flow Data - Core No. 31	66
14	Visco-Inertial Flow Data - Core No. 31	67
15	Viscous Flow Data - Core No. 38	68
16	Visco-Inertial Flow Data - Core No. 38	69
17	Viscous Flow Data - Core No. 45	70
18	Visco-Inertial Flow Data - Core No. 45	71
19	Viscous Flow Data - Core No. 46	72
20	Visco-Inertial Data - Core No. 46	73
21	Viscous Flow Data - Core No. 53	74

continued

Table Number	Title	Page
22	Anomalous Data for Klinkenberg Permeability Core No. 53	75
23	Visco-Inertial Flow Data - Core No. 53	76
24	Viscous Flow Data - Core No. 61	77
25	Visco-Inertial Flow Data - Core No. 61	78

LIST OF FIGURES

Figure Number	Title	Page
1	Permeability Measurement Equipment	14
2	Resistance Measurement Cell	17
2a	Circuit Diagram for Resistance Measurements	19
3	Klinkenberg Permeability Plot with Anomalous Data - Core No. 53	28
4	Klinkenberg Permeability Plot Core No. 53	29
5	Flow Regime Plot - Core No. 53	31
6	Flow Data Plot to Calculate α and β for Core No. 53	32
7	Plot of Log F vs Log Ø (fraction)	45
8	Plot of Log β vs Log $(K)^{0.5}$	37
9	Plot of Log β vs Log Ø (fraction)	38
10a	Plot of Log β vs Log F	46
10b	Plot of Log K vs Log Ø	46
11	Plot of Log f_s vs Log Ø	40
12	Correlation of Inertial Resistance Coefficient (β) with Permeability (K) and Porosity (Ø)	41
13	Plot of Log β vs Log $(\phi^5 . K^{0.5})$	42
14	Plot of Log β vs Log $\left[\phi^5 (KF)^{0.5}\right]$	43
1A	Klinkenberg Permeability Plot Core No. 4X	79
2A	Flow Data Plot to Calculate α and β Core No. 4X	80

continued

Figure Number	Title	Page
3A	Klinkenberg Permeability Plot Core No. 20	80
4A	Flow Data Plot to Calculate α and β Core No. 20	80
5A	Klinkenberg Permeability Plot Core No. 22	81
6A	Flow Data Plot to Calculate α and β Core No. 22	81
7A	Klinkenberg Permeability Plot Core No. 24	82
8A	Flow Data Plot to Calculate α and β Core No. 24	82
9A	Klinkenberg Permeability Plot Core No. 31	83
10A	Flow Data Plot to Calculate α and β Core No. 31	83
11A	Klinkenberg Permeability Plot Core No. 38	84
12A	Flow Data Plot to Calculate α and β Core No. 38	84
13A	Klinkenberg Permeability Plot Core No. 45	85
14A	Flow Data Plot to Calculate α and β Core No. 45	85
15A	Klinkenberg Permeability Plot Core No. 46	86
16A	Flow Data Plot to Calculate α and β Core No. 46	86
17A	Klinkenberg Permeability Plot Core No. 61	87
18A	Flow Data Plot to Calculate α and β Core No. 61	

INTRODUCTION

Fluid flow through porous media may be described by Darcy's law provided the flow is in the viscous region (1). In the case of horizontal laminar flow, the flow rate varies directly as the pressure drop, up to a certain point. Beyond this point, both the proportionality and Darcy's law cease to hold. This point is said to mark the boundary between the viscous and the visco-inertial regions of flow (2).

Horizontal fluid flow in both the viscous and visco-intertial regions may be described by the equation:

$$-\frac{dP}{dX} = \alpha \mu v + \beta \rho v^2 \qquad (1)$$

which is similar to an equation first proposed by Forch-heimer(3). In order that this equation be used to predict pressure distribution for a given flow rate, it is necessary that the coefficients α, μ, β and ρ be known.

The coefficients μ and ρ represent the viscosity and density, both well known fluid properties. As a result they may be evaluated either by measurement or estimation by any of a number of satisfactory methods.

The coefficients α and β are referred to as the viscous and the intertial resistance coefficients. They represent rock properties which are dependent upon the geometry of the porous medium. At present the methods available for measuring and estimating α and β are not entirely

satisfactory. This is due, in part, to the fact that a means of adequately describing the geometry of a porous system is not available and that the exact relationship between the geometry and the coefficients α and β is not yet known.

Since α is the inverse of the rock property, permeability, it may be evaluated from flow test using the Darcy's law, provided flow is restricted to the viscous region. The inertial resistance coefficient can only be determined experimentally by observing flow in the visco-intertial region, and employing equation (1), or a modification thereof. The modified form of this equation that is commonly used, may be written in the form proposed by Green and Duwez(4).

$$\frac{\Delta (P^2)\ M\ g_c}{2\ (ZRT)\ L\mu G} = \alpha + \beta \left(\frac{G}{\mu}\right) \qquad (2)$$

Although this method is adequate for research work, it is considered too difficult for routine core analysis. To circumvent difficulty various attempts have been made to relate β to other rock properties which lend themselves more readily to evaluation through routine core analysis, e.g. porosity, permeability etc. The first such attempt was reported by Cornell and Katz(5) who correlated β with permeability. Janicek and Katz(6) improved the correlation by including porosity as a parameter. Finally Hamilton(7) extended the correlation and presented a new expression for β as a function of permeability and porosity.

An examination of the three correlations indicates that they are dimensionally inconsistent and that they are based on the Kozeny model(8). Since a dimensionally inconsistent correlation does not seem reasonable and the Kozeny model does not admit to inertial effects, the object of this study was to examine the interrelationships of the inertial resistance coefficient, permeability, tortuosity, porosity and the formation resistivity factor, with the view of developing a correlation free of the two above-mentioned objections.

This study was restricted to an examination of the data of previous workers, the undamaged rock specimens studied by Hamilton(7) and a group of ten new specimens. The new specimens were selected to provide a wide range of porosity and permeability.

THEORY

Flow Through Porous Media

Flow of liquids through porous media was first described by Darcy(9) in 1856 by the equation

$$q = -c \frac{dh}{dl} \tag{3}$$

Although this equation had been modified and used in the petroleum industry during the early 1930's it was first rigorously examined by Hubbert(10) in 1940. For the case of horizontal flow, he showed that

$$q = -\frac{K}{\mu} \frac{dP}{dl} \tag{4}$$

This form of the equation was found to be satisfactory for low flow rates of liquids. However in order that the equation be applied, K and μ had to be known. For application to oil reservoirs, it became the practice to subject small rock samples to flow tests and apply Darcy's law to evaluate the permeability, K.

Since flow tests using liquids as the flowing fluid proved difficult, it seemed appropriate to use a gas instead of a liquid. This seemed proper since it had been shown that K was a property of the porous medium. For this purpose it was shown that Darcy's law could be written as

$$q_m = -\frac{K}{2\mu P_m} \frac{d(P^2)}{dl} \tag{5}$$

The actual application of this method for obtaining K was found difficult since even for low flow rates K varied with pressure. Klinkenberg(11) examined this phenomenon and showed that, whereas with liquids there was no appreciable slip at the wall, this was not true for gases. He observed that when the mean free path of the molecules of a gas approaches the size of the flow channel, slip at the wall becomes appreciable. He went on to show that apparent or observed permeability, K_a varied linearly with the inverse mean pressure, P_m.

He proposed that since,

$$K_a = K \left(1 + \frac{b}{P_m}\right) \qquad (6)$$

a plot of K_a versus $1/P_m$ would yield the equivalent liquid permeability when extrapolated to the point $\frac{b}{P_m} = 0$

Subsequent to Klinkenberg's observations, it became standard practice to obtain K from such a plot. The permeability value so obtained was denoted by K_∞ and referred to as the Klinkenberg permeability.

The procedure consisted of conducting flow tests by varying the upstream pressure and maintaining the downstream pressure at atmospheric conditions. This procedure, often times resulted in data which did not yield a linear relationship.

Several attempts were made to eliminate the slip effect by maintaining it at some fixed value(12). However,

Hamilton(7) observed that although such a practice would allow reproducibility, different values of mean pressure yielded different permeabilities.

Much earlier, it had been observed with liquid flow that Darcy's law failed at high flow rates. This deviation from Darcy's law was attributed to turbulence by most observers; whereas, Hubbert(10) attributed it to inertial effects and Houpeurt(13) proposed expansion and contraction of the fluid during its flow along the pore channels, as the cause.

In order to describe flow over a wide range of flow rates Green and Duwez(4) suggested the equation

$$-\frac{dP}{dL} = \alpha \mu v + \beta \rho v^2 \qquad (7)$$

which is similar to an equation first proposed by Forchheimer(3). For the particular case of gas flow, they reasoned that if $\rho v = G =$ constant, then the equation could be written as

$$-\frac{M g_c}{2(ZRT)} \frac{d(P^2)}{dL} = \alpha \mu G + \beta G^2 \qquad (8)$$

or as

$$\frac{\Delta (P^2) M g_c}{2L (ZRT) \mu G} = \alpha + \beta \left(\frac{G}{\mu}\right) \qquad (9)$$

in the integrated form.

A similar result was obtained by Cornell and Katz(5). They considered the deviations from Darcy's law to be the result of turbulence. Using a Kozeny type equation(14) in

terms of effective pore diameter (D_E) and tortuosity τ, they developed the equation

$$\frac{\Delta (P^2)\ g_c}{L} = \left(\frac{32F}{K_1 D_E^{\,2}}\right) \mu \frac{2ZRT}{M} G + \left(\frac{32F^{1.5}}{K_2 D_E^{\,0.5}}\right) \frac{2ZRT}{M} G^2 \qquad (10)$$

The factors K_1 and K_2 were termed as geometrical constants, and had to be determined for each porous medium. The constant K_1 was closely related to the Kozeny constant(14) and was assumed to equal 0.5. The factor K_2 was correlated with the relative roughness ϵ, as in the case of pipes. They assumed that some sort of correlation must exist between K_2 and ϵ, since the latter is characteristic of a porous medium.

A comparison of equations (9) and (10) shows them to be identical, provided that,

$$\alpha = \left(\frac{32F}{K_1 D_E^{\,2}}\right) \qquad \text{and} \qquad \beta = \frac{32F^{1.5}}{K_2 D_E \phi^{0.5}} \qquad (11)$$

Initially these equations were of academic interest only. However an examination of certain natural gas reservoirs showed that at high delivery rates, flow in the reservoir was in the visco-inertial region. These equations then became important in the study of such reservoirs. In order to make such studies values of the inertial resistance coefficient β had to be known. Although β could be obtained experimentally, techniques were sought, for estimating β from other parameters.

In the earliest such attempt Cornell and Katz(5) proposed the correlation

$$\beta = \frac{4.11 \times 10^{10}}{K^{1.33}} \qquad (12)$$

Subsequently Janicek and Katz(6) re-examined the data of Cornell and observed that

$$F\emptyset = 4 \qquad (13)$$

By assuming $K_1 = 0.5$, and noting that $F\emptyset = 4$ and $K = \frac{9.411 \times 10^{13}}{\alpha}$ they showed that

$$D_E = \frac{8(FK)^{0.5}}{9.7 \times 10^{6}} \qquad (14)$$

by virtue of equation (11).

Sensing that the factor K_2 was related to $\emptyset$ and K they plotted K_2 versus $K/\emptyset$ and expressed the best fit by

$$K_2 = 2.82 \times 10^{-2} \left(\frac{K}{\emptyset}\right)^{0.75} \qquad (15)$$

Finally substituting for D_E, F and K_2 in equation (11) they obtained the expression

$$\beta = \frac{5.5 \times 10^{9}}{K^{1.25}\ \emptyset^{0.75}} \qquad (16)$$

which they proposed as a general correlation(15).

Hamilton(7) observed that the Janicek and Katz correlation did not agree well with experimental data. He therefore obtained additional data and on the basis of these

along with those of Cornell he proposed that

$$K_2 = 5.62 \left(\frac{K\phi}{F}\right)^{0.63} \tag{17}$$

which when substituted into equation (11) yielded the expression

$$\beta = \frac{6.6 \times 10^7}{K^{1.13} \phi^{2.76}} \tag{18}$$

He proposed this as a general correlation.

Electrical Properties of Porous Media

The electrical properties of a rock depend upon the geometry of the voids and the fluids which fill them. The use of such properties to characterize reservoir rocks was first suggested by Archie(16). Amongst other things he defined the formation resistivity factor as

$$F = \frac{\text{Resistivity of a saturated medium}}{\text{Resistivity of the saturating solution}}$$

This factor, is a parameter which reflects the influence of pore geometry on electrolytic conduction through the medium. It in effect combines porosity and tortuosity into one parameter.

Since resistance of a saturated medium may be expressed as

$$R_c = \rho_b \frac{L_e}{(\phi A)} \tag{19}$$

and since the resistance of a congruent volume of the saturating fluid, may be written as

$$R_b = \rho_b \frac{L}{A} \tag{20}$$

then by definition

$$F = \frac{(\rho_b L_e)/(\emptyset A)}{(\rho_b L)/A}$$

$$= \frac{L_e/L}{\emptyset} \tag{21}$$

However, the square of the ratio of the tortuous average length of the pore channels traversed by the current flowing from one to the other of the parallel planes within the saturated medium to the distance of the two planes, has been defined(17) as the tortuosity of the medium. Therefore, the formation resistivity factor may be expressed as

$$F = \frac{\tau^{0.5}}{\emptyset} \tag{22}$$

Wyllie and Rose(18) concluded that the hydraulic and electrical tortuosities in a porous medium are extraordinarily close and, for all purposes could be considered identical.

Archie(16) correlated the observed formation resistivity factor with porosity and permeability. He

suggested that the correlation with ϕ was the better correlation and that the formation resistivity factor could be expressed as

$$F = \phi^{-m} \tag{23}$$

where m is the cementation factor. He further reported that m probably ranged from 1.8 to 2.0 for consolidated sandstones.

Winsauer(19) reported a similar relationship based on correlations of their data from a large number of sandstone cores. This equation, commonly referred to as the Humble equation(20) is

$$F = 0.62\,\phi^{-2.15} \tag{24}$$

At present it is best to say that the formation resistivity factor is a function of porosity and some unknown effect of the complex internal geometry of the porous medium. Winsauer and Shearin (19) and Wyllie and Spangler(17) have summarized the pertinent literature on this aspect.

EXPERIMENTAL EQUIPMENT

It was decided to obtain data for the inertial resistance coefficient, porosity, permeability and formation resistivity factor on ten cores used by Hamilton(7) as well as an additional set of ten selected core samples. To accomplish this, various pieces of equipment were necessary.

Sample Preparation Equipment

The equipment used to prepare the rock specimens for porosity and flow measurements was identical to that used by Hamilton(7). In order to prepare the specimens for resistance measurements, a gram-atic balance, a vacuum jar, a mechanical vacuum pump and a de-aerated 50,000 p.p.m. brine solution were used.

Porosity Measurement Apparatus

A modified Oilwell Research Porosimeter(21) using helium was employed to obtain data on grain volume. An electric Mercury Pycnometer(18) was used to obtain data on the bulk volume of the samples. Both these pieces of equipment were calibrated prior to use by means of six solid blanks of known dimensions.

Permeability Measurement Apparatus

Several method for holding small rock samples for the purpose of measuring permeability are described in the literature(5)(22)(23). Hamilton(7) modified the method described by Johnston and Taliaferro(23) and employed a core holder machined from mild steel stock. In this work, the same core holder was employed. A line diagram of the permeability measurement apparatus is shown in figure 1.

The core holder consisted of two pressure taps in the body (upstream and downstream), and two end plates with O ring seals. Each end plate was provided with a threaded pressure fitting, and an Iron-Constantan thermocouple.

A sleeve was made for each core using an extra long No. 26 rubber stopper. Each stopper was drilled to a diameter 0.1 inch less than the diameter of the core for which it was intended. This provided for a squeeze fit of the core into the sleeve. The sleeve containing the core was placed into the tapered section of the core holder, followed by a sliding metal follower and a SKF No. 51105 thrust bearing. These were held in place by screwing down a metal follower.

Nitrogen was used as the flowing fluid. The inlet flowing pressure was regulated at the gas cylinder by means of a 3000/200 p.s.i. regulator for low pressures and a 3000/3000 p.s.i. regulator for pressures in excess of 200 p.s.i. From the regulator the gas was passed through a 0.25 inch

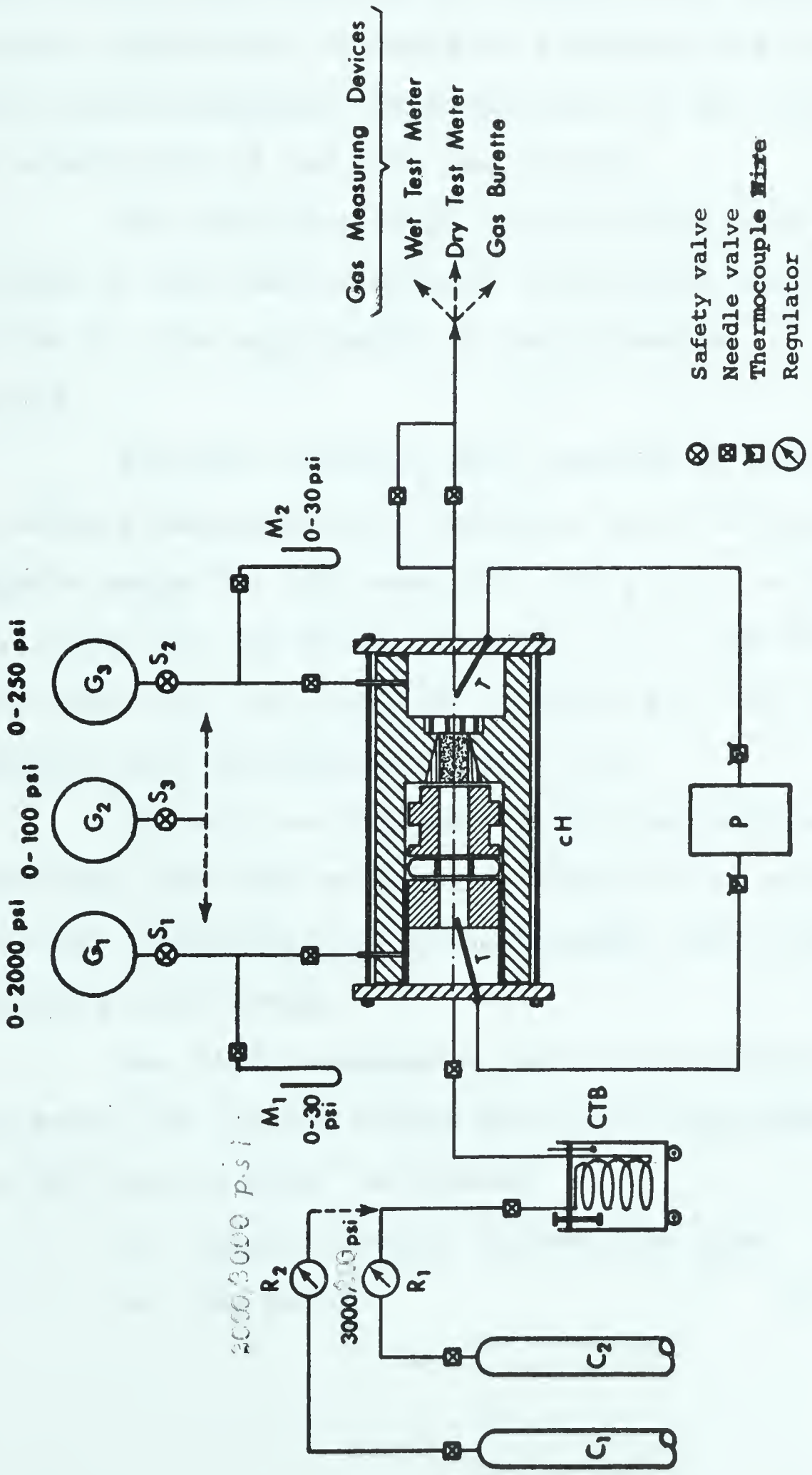

Permeability Measurement Apparatus

Figure 1

diameter soft copper tubing and then admitted to the core holder through a 0.125 inch stainless steel tubing. The copper tubing was immersed in a glycol bath, maintained at a constant temperature by means of a heating and refrigeration unit, so as to control the temperature of the flowing fluid. The sensitivity of the bath was $\pm$0.5°F.

Two stainless steel needle valves were arranged in parallel on the downstream side of the core holder to provide for the application of back pressure, if and when desired.

Pressure readings were obtained by means of water and mercury manometers for pressures up to 30 p.s.i., a Seeger's gauge for the range 30 - 100 p.s.i., a 250 p.s.i. Heise gauge for the range 100 - 250 p.s.i. and 2000 p.s.i. Heise gauge for the range 250 - 2000 p.s.i. All these instruments were calibrated prior to use.

Flowing gas temperatures at the upstream and downstream ends were measured by means of the previously mentioned Iron-Constantan thermocouples, and a Leeds and Northrup potentiometer.

Gas flow measurements were made using an electric stop watch and various volume measuring instruments, depending upon the rate of flow, as follows:

a. Selas Porcelain Microfilter tube $0 < Q \leq 0.5$

b. Gas Buret $0.5 \leq Q \leq 2$

c. Wet Test Meter $2 \leq Q \leq 20$

d. Diaphragm Meter $20 \leq Q \leq 120$

where Q is the rate of flow in ft^3/hr.

Resistance Measurement Apparatus

An apparatus for measuring resistance of small rock samples is described in the literature by Rust(24). A modified version of his apparatus was found more appropriate for this investigation. The apparatus consisted of a lucite housing, split into similar halves, which could accomodate the rock sample. Two sets of six, solid silver, platinum tipped, potential electrodes, under spring tension were seated in the housing in such a way that when the core was in place, the electrodes were distributed along the circumference of the core sample. Two brass discs were used as current electrodes. They were arranged to make contact with the two ends of the core sample through brine saturated felt pads. The pads were threaded with thin silver wire to ensure electrical contact between the brass discs and the core.

The lucite housing and the brine saturated core were housed in a lucite box, partially filled with 50,000 p.p.m. brine to minimize evaporation while the test was in progress.

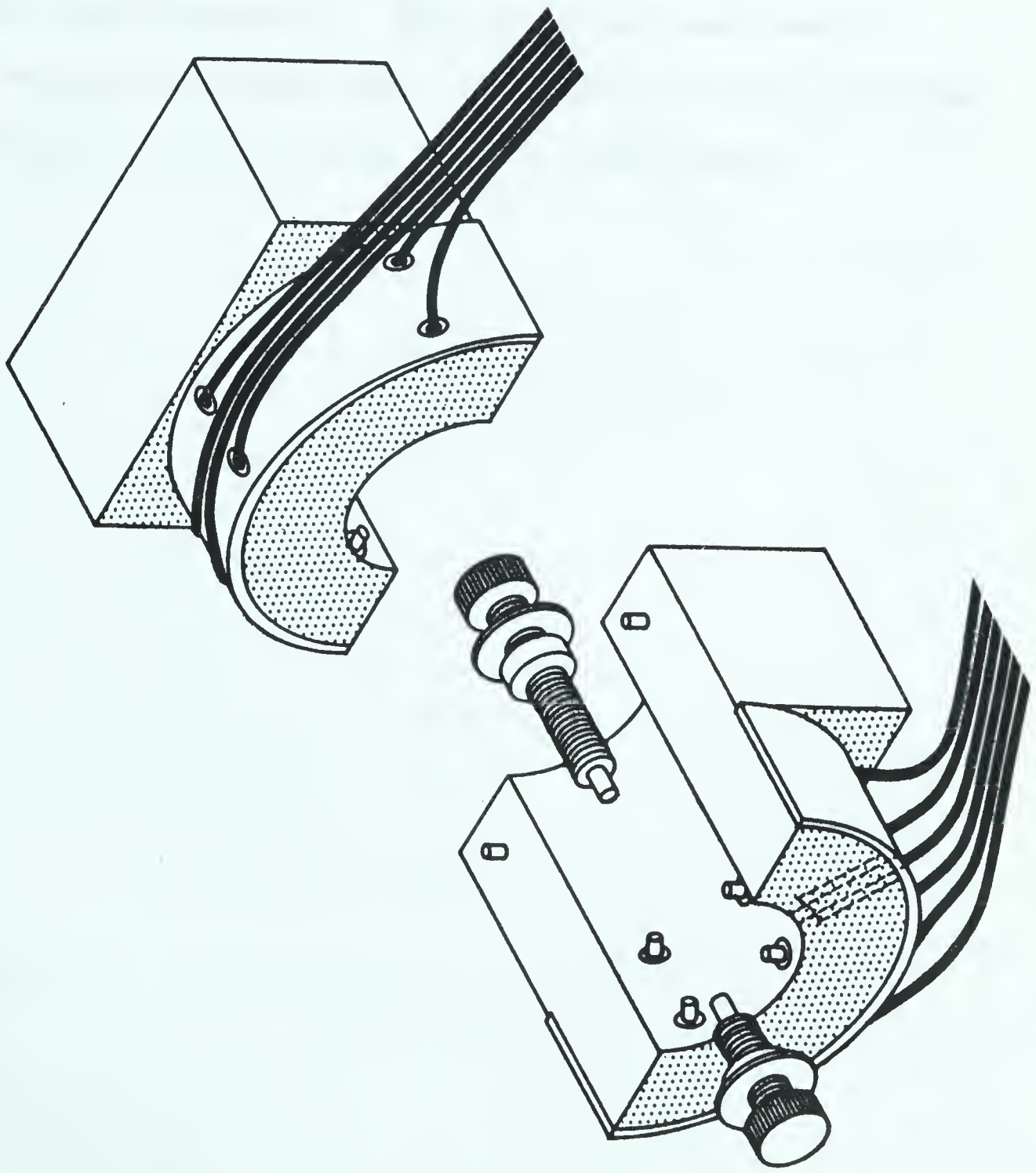

Figure 2. Resistance Measurement Cell
(after Rust(24))

The wiring of the apparatus was of the permanent type as shown by the line diagram in Figure 2a. Two selector switches provided for resistance measurements by either the two electrode or the four electrode method.

Dunlap's(25) check, for contact resistance developed at the current electrodes, was incorporated by including a series resistor equal in value to the input impedance of the vacuum tube voltmeter. The voltmeter used was a Hewlett Packard model 400 AB. The input line was shielded so as to minimize the effect of background noise.

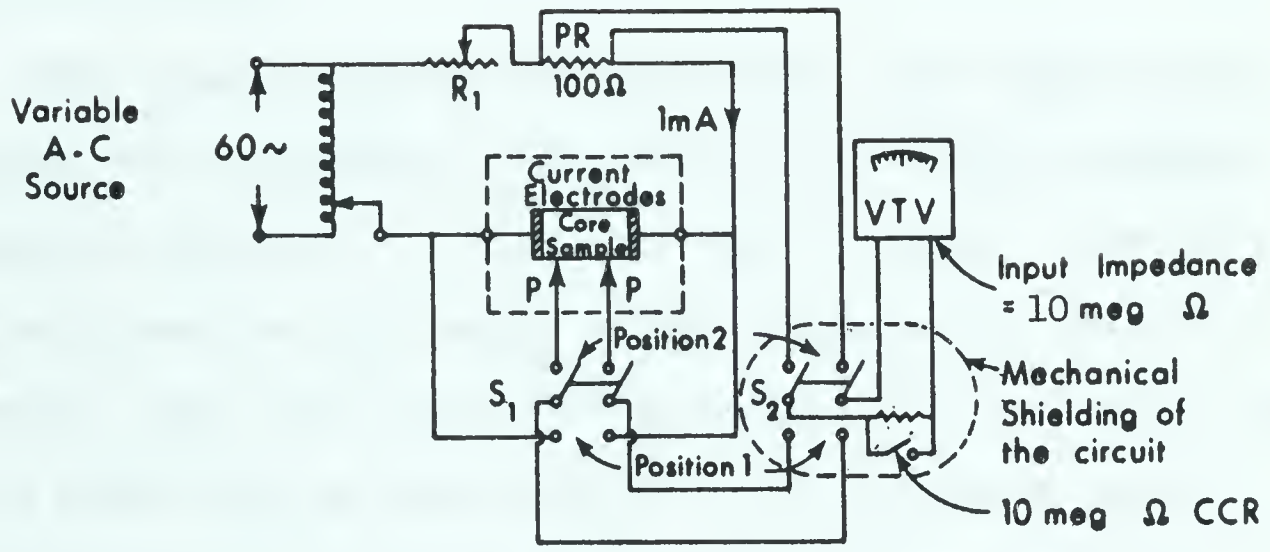

R_1 50,000 Ω , adjustable resistor

PR 100 Ω ; precision resistor

VTV A-C vacuum tube voltmeter

ccR contact check resistor; 10 meg Ω

PP Potential probes

S_1 Selector switch 1

S_2 Selector switch 2

Figure 2-a. Circuit Diagram for Resistance Measurements (after Rust(24))

EXPERIMENTAL PROCEDURE

In addition to ten cores used by Hamilton(7), ten new cores were selected for observation. The selection was such as to provide a wide range of porosity (2% - 27.5%) and permeability (0.000125 md to 1160 mds).

Sample Preparations

Each small cylindrical reservoir rock sample was cut parallel to its bedding plane using a one-inch diamond drill, and was limited in length to three inches. Since it was observed that the end pores became plugged due to the sawing action, new end faces were produced by fracturing, using the device described by Hamilton(7). The fractured cores were approximately 1.5 inches in length and one inch in diameter.

The physical dimensions of the cores were obtained by means of a micrometer caliper. The effective diameter of each core was taken to be the average of five readings and the effective length as the average of seven readings.

The cores were extracted by means of a Soxhlet apparatus using benzene as the solvent. After an extraction period of about 18 hours, the cores were allowed to soak over night in fresh benzene. If, after this period, the benzene was found to be clear, it was inferred that the

extraction was complete. If, however, the benzene was oil-stained, the procedure was repeated. Subsequent to satisfactory extraction, the cores were dried in a constant temperature oven at 200°F for about 12 hours. The cores were allowed to cool to room temperature and were then stored in a dessicator until used.

Porosity Measurements

The data on matrix volume of the cores were obtained using the modified Oil Well Research Porosimeter(21). The data on bulk volume were obtained using an electric mercury Pycnometer(18). Six steel blanks and six lucite blanks of known dimensions were used to calibrate the porosimeter and the pycnometer, respectively. From these data, the porosity values were computed and recorded in Table 1. The observations were made according to standard procedures, therefore, no further details are given here.

Permeability Measurements

Each core housed in its rubber sleeve was placed in the tapered section of the core holder. The sleeve was slightly greased on the outside to facilitate loading and to prevent fluid bypass during test. The follower was screwed down tightly and the end plates were assembled by tightening

Table 1

Physical Properties and Porosity Data

Source	Core No.	Formation	Rock Type	Core Diameter (inch)	Effective Length (inch)
Hamilton	3	Cardium	Sandstone	0.998	1.490
Hamilton	4	Cardium	Sandstone	0.997	1.461
Hamilton	5	Cardium	Sandstone	0.996	1.462
Hamilton	7	Sturgeon Lake	Limestone	0.996	1.498
Hamilton	8	Berea	Sandstone	0.996	1.474
Hamilton	10	Blairmore	Basal Quartz	1.015	1.445
Hamilton	11	Blairmore	Basal Quartz	1.015	1.341
Hamilton	12	Viking	Sandstone	1.015	1.414
Hamilton	13	Viking	Sandstone	1.016	1.467
Hamilton	14	Belly River	Sandstone	1.015	1.480
C & G Lab**	4X	Cardium	Sandstone	0.9820	1.4931
C & G Lab.	20	Belly River	Sandstone	0.9860	1.4760
C & G Lab.	22	*	Sandstone	0.9934	1.5292
C & G Lab.	24	*	Sandstone	0.9996	1.5746
C & G Lab.	31	Belly River	Sandstone	0.9880	1.5100
C & G Lab.	38	*	Sandstone	0.9934	1.5770
C & G Lab.	45	Taber	Sandstone	0.9900	1.526
C & G Lab.	46	Taber	Sandstone	1.0000	1.5601
C & G Lab.	53	Taber	Sandstone	0.9934	1.5598
C & G Lab.	61	Taber	Sandstone	0.9996	1.5922

* Unknown
** The Chemical and Geological Laboratories, Edmonton

Table 1 - continued

Core No.	Bulk Volume (cc)	Pore Volume (cc)	Ø %	Area $in.^2$	Effective Length (L) / Area (A)
3	19.094	3.593	18.82	0.782	1.9054
4	18.690	3.945	21.11	0.781	1.8707
5	18.664	3.202	17.16	0.779	1.8768
7	19.150	2.605	13.60	0.780	1.9205
8	18.806	3.646	19.39	0.778	1.8946
10	19.165	3.825	19.96	0.810	1.7840
11	17.793	3.628	20.39	0.810	1.6556
12	18.757	1.842	9.82	0.810	1.7457
13	19.472	2.002	10.28	0.810	1.8111
14	19.629	3.701	18.85	0.810	1.8272
4X	18.82	4.17	22.18	0.7574	1.9712
20	18.28	0.42	2.30	0.7636	1.9329
22	18.95	4.60	24.33	0.7775	1.9668
24	19.77	4.28	20.91	0.7848	2.0064
31	18.50	1.08	5.84	0./667	1.9695
38	19.32	4.50	23.36	0.7775	2.0026
45	18.10	3.90	21.55	0.7698	1.9823
46	19.68	3.73	18.10	0.7854	1.9864
53	19.47	5.05	22.06	0.7775	2.0062
61	19.87	5.69	27.43	0.7848	2.0288

the five threaded steel bolts provided for that purpose.

The core holder assembly and the connections were tested for gas leakage by pressuring to 1800 p.s.i. and using standard soap solution. The soap solution was examined for bubbles by means of a magnifying lens. Any leaks that were detected, were removed by coating the area with Lepage's glue.

Nitrogen at a regulated pressure and temperature was admitted into the core. The downstream end pressure and the flow rate was measured using instruments previously mentioned. In accordance with the Klinkenberg theory(11), the flow rate was limited to the viscous flow region by applying the desired amount of back pressure. The temperatures of the gas at the upstream and the downstream ends were observed and recorded.

Several readings were taken at various mean pressures, and the corresponding flow rates were noted. Three flow rate readings were taken for each data point to make sure that stabilized flow was attained. Whenever the upstream pressure was changed, a stabilization period of from 15 - 20 minutes was provided.

Visco-Inertial Flow Measurements

Since visco-intertial flow was desired, back pressure was not applied. As in the case of the permeability measurements, three readings were taken for each data point.

Sample Preparations for Resistance Measurements

The clean dry cores were first weighed. Then they were evacuated to 0.15 mm of mercury by means of a vacuum pump. A de-aerated 50,000 p.p.m. sodium chloride solution (prepared by adding pure sodium chloride to freshly boiled distilled water) was slowly admitted into the vacuum jar until all the cores were submerged in the solution. The cores were then allowed to remain in the submerged condition for 12 hours.

The saturated cores were weighed. This was done by placing the saturated cores on a saturated felt pad so as to minimize the loss of brine by drainage. Using these data, the saturations were calculated, as given in Table 4.

Resistance Measurements

A schematic wiring diagram of the resistance measuring circuit is given in figure 2a. With the core sample mounted in the lucite housing, the current flowing through the core was set at one milliampere by adjusting the voltage drop across the wire wound precision resistor. Manipulation of switches I and II permitted voltage drop measurements to be made, either across the entire core sample (two electrode method) or across a portion of the sample (the four electrode method).

The current electrodes were checked for contact resistance by Dunlap's method(25). If and when such resistance was found to be present, it was removed by re-saturating the felt pads and re-making of the current electrode contacts. Subsequent to the removal of contact resistance, three readings were taken on each core by each of the two methods.

The resistivity of the brine was measured periodically by means of a standard conductivity bridge.

DISCUSSION OF EXPERIMENTAL RESULTS

The data on porosity, permeability, formation resistivity factor and tortuosity were obtained using the techniques outlined elsewhere in this work.

The permeability data were obtained by applying back pressure to limit the flow rates to the viscous region. This was found necessary because anomalous values of Klinkenberg permeability, which were at least 100% lower than the true Klinkenberg permeability, were obtained if the required amount of back pressure was not applied.

It is a common practice to plot a set of $1/P_m$ values against corresponding values of apparent permeability, K_a, and to extrapolate the straight line portion to $\frac{1}{P_m} = 0$, to give the Klinkenberg permeability. It is also usual to regard the straight line portion of the plot to indicate absence of the slip effect, and any deviation from the straight line to indicate the slip phenomenon.

This study has indicated that this criterion does not always hold ture. Data on core No. 53 have been included here to elaborate this statement. A comparison of Figures 3 and 4 shows that the Klinkenberg permeability evaluated from data obtained without application of back pressure is 175 mds, and 375 mds when evaluated from data taken when back

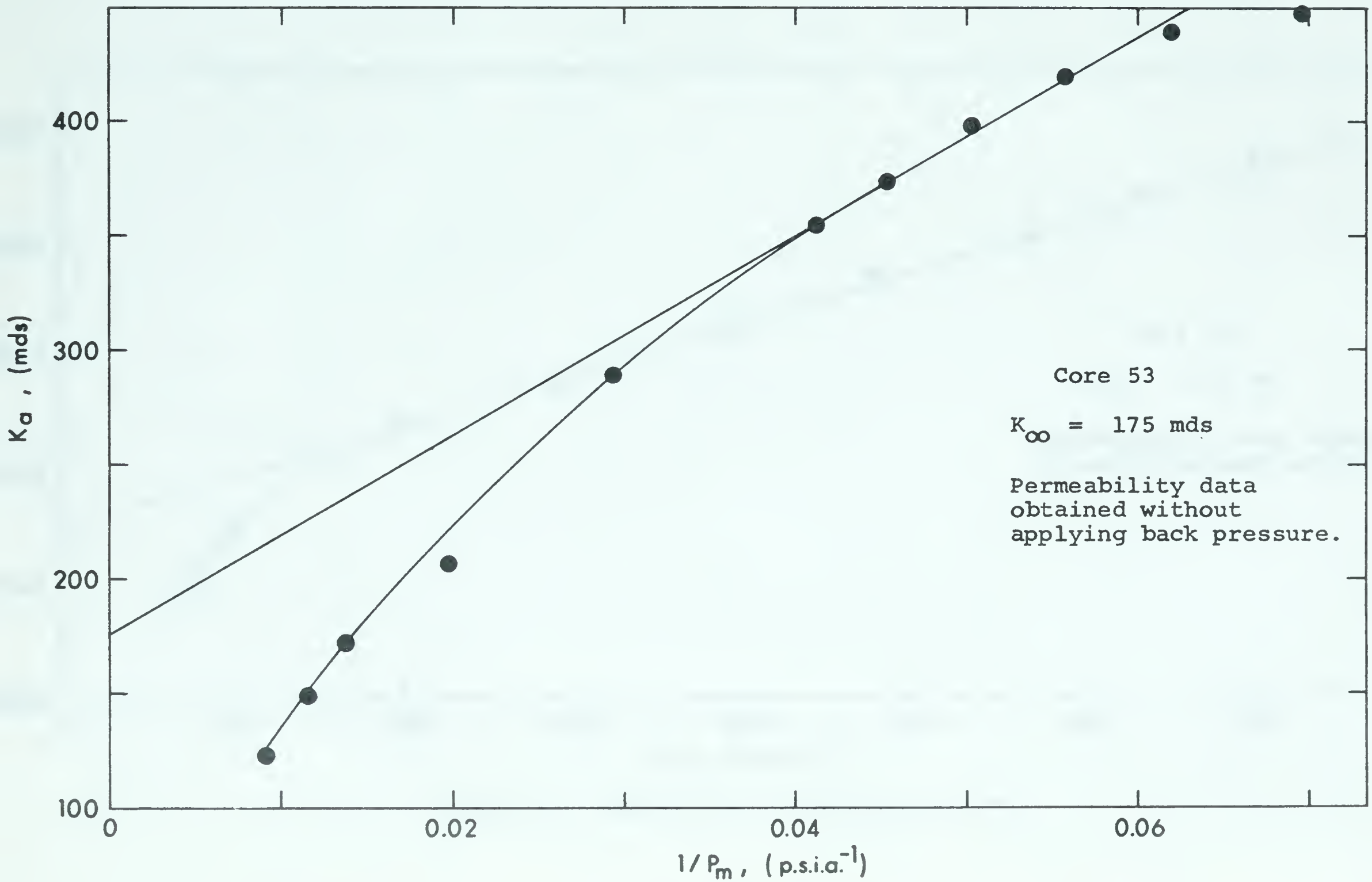

Figure 3. Klinkenberg Permeability Plot

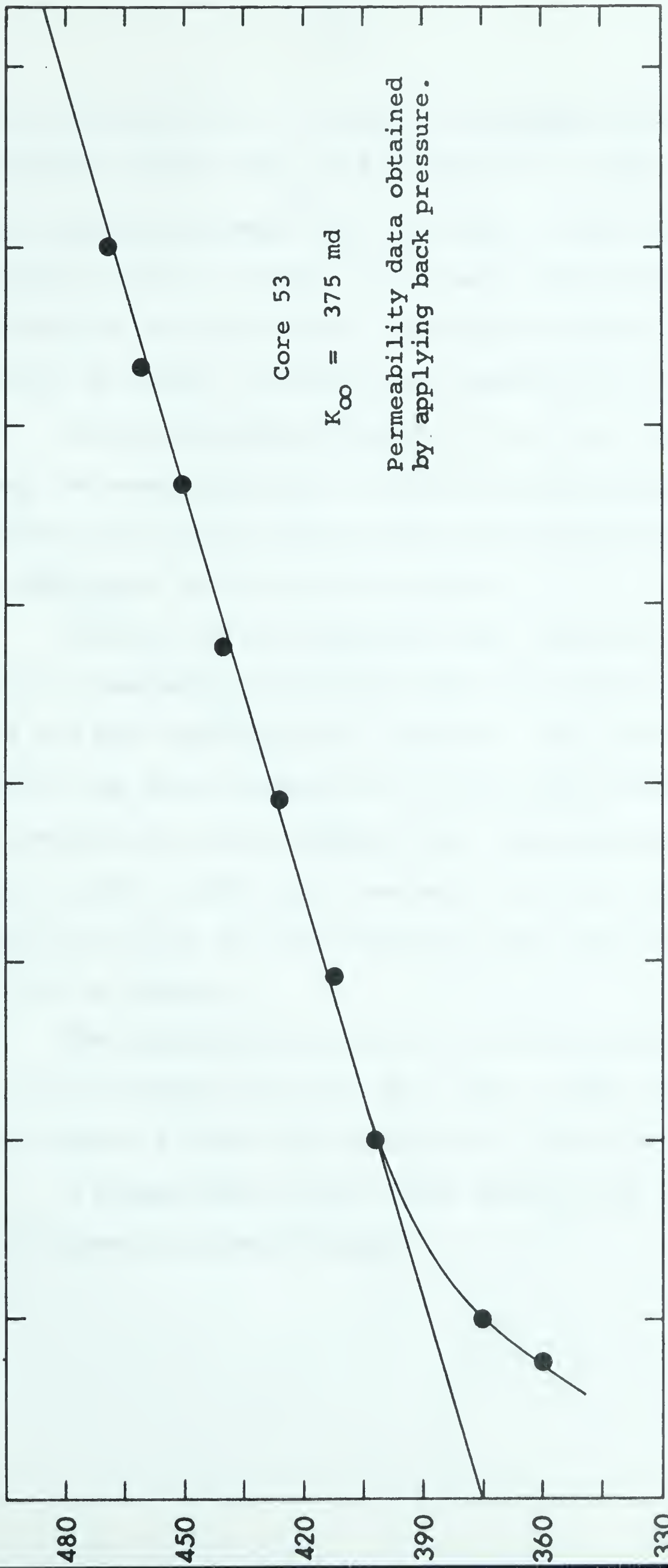

Figure 4. Klinkenberg Permeability Plot

pressure was applied. In Figure 3 a straight line portion is indicated for values of $\frac{1}{P_m} \geqslant 0.04$ (psia)$^{-1}$. This, however, does not necessarily mean that the data in this range are in the viscous region. In fact it is very likely that these points are not in the viscous region since points of equal $1/P_m$ value in Figure 4 yield higher permeability values.

It was therefore decided to use only viscous flow readings for evaluating the Klinkenberg permeability. This was achieved by taking numerous data and selecting only those which were in the viscous region.

Katz et al(15) suggested that a plot of $\Delta(P^2)$ versus Q should be adequate to represent the flow data in both the viscous and the visco-inertial regions. The straight line portion of the plot represented viscous flow and any deviation from the line indicated the visco-inertial flow region. A plot of this type was made for each core. The viscous flow region was determined in each plot as is shown for core 53 in Figure 5.

The permeability data were also evaluated using the α values obtained from the flow data in the visco-inertial region. Figure 6 shows the permeability value so obtained.

A comparison of the values obtained by these two techniques is shown in Table 2.

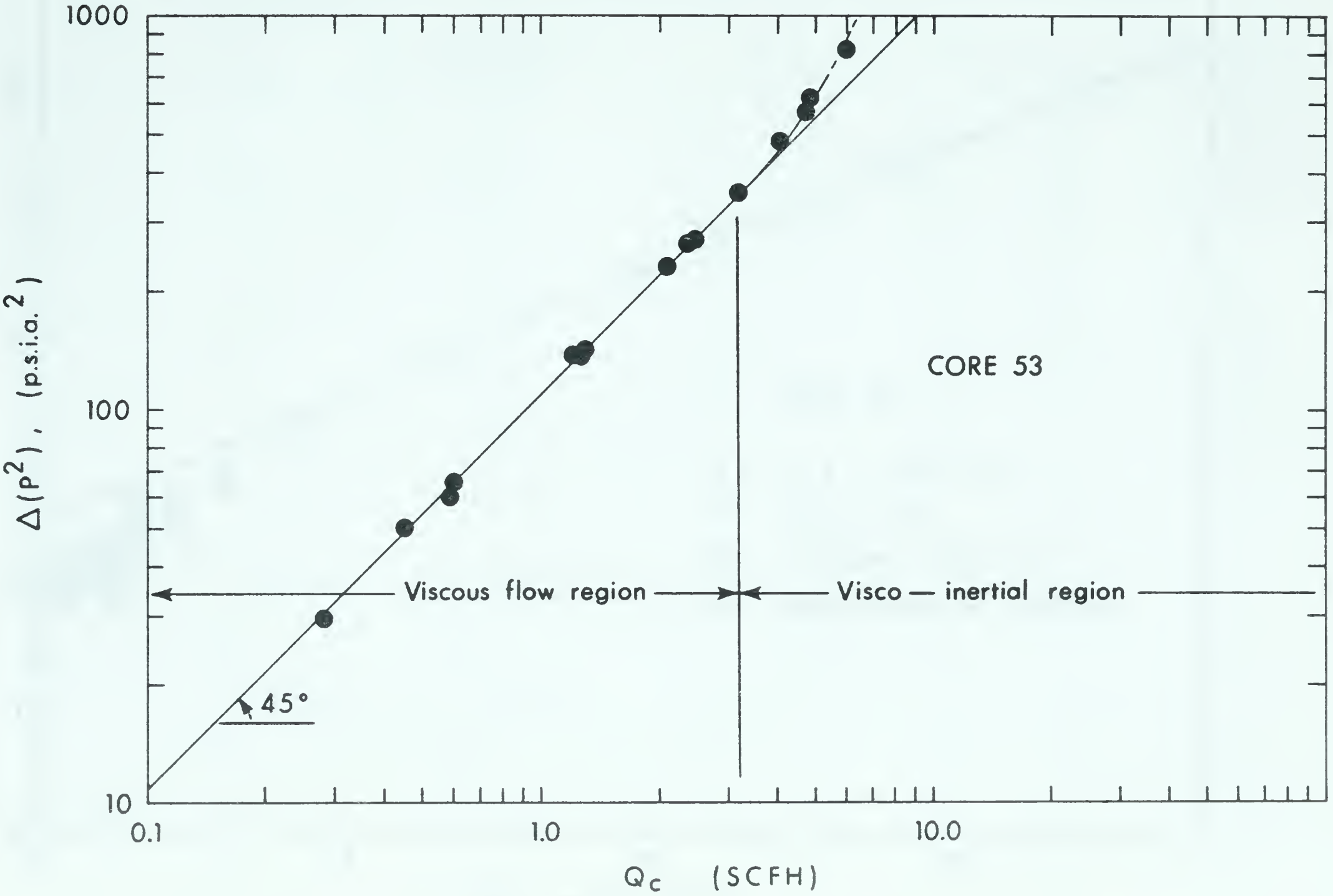

Figure 5. Flow Regime Plot

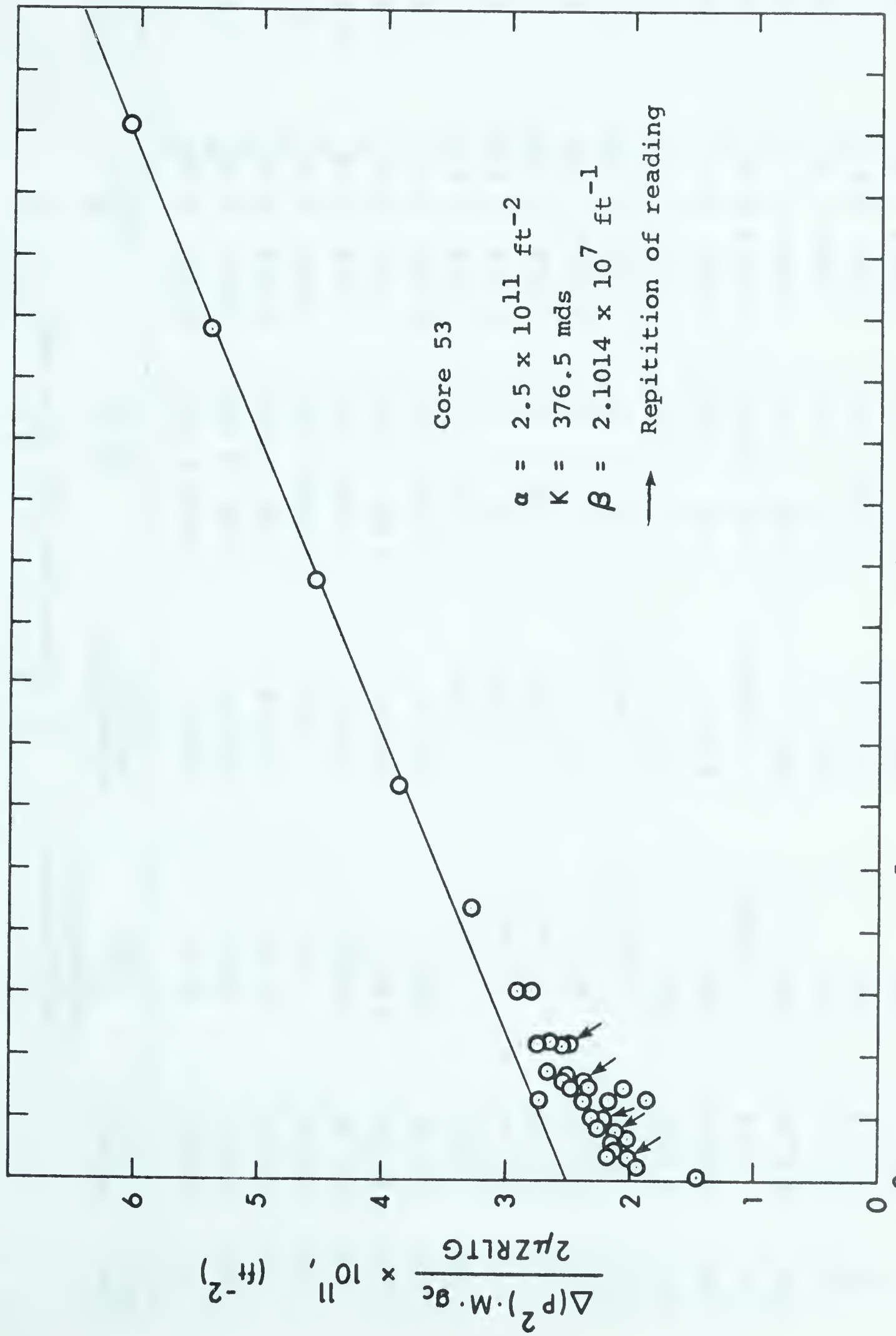

Figure 6. Flow Data Plot to Calculate α and β

Table 2

Summary of Porosity, Permeability and Inertial Resistance Coefficient Data

Core No.	Porosity %	Klinkenberg Permeability K_∞ (md)	Visco-inertial flow data: Permeability ** (md)	α (ft^{-2})	β (ft^{-1})	Deviation %
3*	18.82	17.2	16.61	5.665×10^{12}	2.533×10^{8}	3.55
4*	21.11	27.0	29.59	3.18×10^{12}	1.85×10^{8}	- 8.75
5*	17.16	17.9	17.96	5.24×10^{12}	2.165×10^{8}	- 0.33
7*	13.60	1.6	1.32	7.125×10^{13}	1.807×10^{10}	21
8*	19.39	179.0	163.81	5.745×10^{11}	1.144×10^{7}	+ 9.27
10*	19.96	240.0	244.44	3.85×10^{11}	1.107×10^{7}	- 1.82
11*	20.39	403.5	415.50	2.265×10^{11}	5.689×10^{6}	- 2.89
12*	9.82	0.22	0.197	4.778×10^{14}	1.962×10^{11}	11.67
13*	10.28	0.565	0.574	1.64×10^{14}	3.417×10^{10}	- 1.57
14*	18.85	0.643	0.600	1.568×10^{14}	1.264×10^{10}	7.17
4X	22.18	56.4	57	1.65×10^{11}	5.2184×10^{7}	- 1.1
20	2.30	0.000125	0.000171	5.50×10^{17}	5.9527×10^{16}	-27
22	24.33	840	855.7	1.10×10^{11}	7.7174×10^{6}	- 1.9
24	20.91	366	376.5	2.50×10^{11}	3.361×10^{7}	- 2.8
31	5.84	0.00375	0.00377	2.50×10^{16}	3.1372×10^{13}	- 0.4
38	23.36	1040	1069.7	8.80×10^{10}	7.3489×10^{6}	- 2.8
45	21.55	455	473	1.99×10^{11}	1.9088×10^{7}	- 3.8
46	18.10	82	83.45	1.128×10^{12}	3.900×10^{8}	- 1.74
53	22.06	375	376.5	2.5×10^{11}	2.1014×10^{7}	- 0.4
61	27.43	1160	1162.1	8.1×10^{10}	4.3173×10^{6}	- 0.2

* Hamilton's work - reference (7), except Klinkenberg permeability data which was obtained by the author

** Permeability $K = \dfrac{9.413 \times 10^{13}}{\alpha}$

Figures 1A to 18A in Appendix II show the permeability values obtained by the above-mentioned techniques.

In order to arrive at a general correlation between the inertial resistance coefficient and the reservoir rock properties, Hamilton's data(7) and Cornell's data(14) were also included in this work. An examination of Figures 12, 13 and 14 shows that scatter of Cornell's data is more than either Hamilton's work or this work. There is reason to question the accuracy of Cornell's data.

In order to obtain values of porosity, Cornell saturated his samples with distilled water. Such a technique will yield results of questionable accuracy for two reasons. First, porosity determination by liquid saturation is inherently inaccurate since complete saturation is difficult to attain as may be seen from Table 4, Appendix 1. Second, it is a well known fact that the introduction of distilled water into a natural porous medium will cause swelling of argillaceous impurities, thereby altering both the porosity and permeability.

The permeability values used by Cornell were calculated from α values only and were not checked by the Klinkenberg method.

An examination of Equations 12, 16 and 18 representing the correlations proposed by Cornell and Katz(5), Janicek and Katz(6) and Hamilton(7) showed that they are based on a modification of Kozeny's model(14) for porous media. The Kozeny model assumes a rectilinear system of pore channels, and thus cannot account for the effect of inertial forces,

which develop because of a curvilinear system of pore geometry (10)(13). Also, those correlations are dimensionally inconsistent because β (ft^{-1}) cannot be equated to K (ft^2). In view of these objections the very basis of the correlations was re-examined.

The internal resistance coefficient β is known to depend on the pore geometry of a porous medium. Parameters such as $\emptyset$, K, F, S_A, τ, etc. characterize the pore geometry. Intuitively therefore, a relationship must exist between β and the reservoir parameters. This relationship may be expressed mathematically as

$$\beta = f_1 \text{ (pore geometry)}$$

where f_1 denotes some function.

and

$$\text{pore geometry} = f_2 \ (\emptyset,\ K,\ F,\ \tau,\ S_A,\ \text{etc})$$

where f_2 is some function.

Therefore,

$$\beta = f_1 \left[f_2 \ (\emptyset,\ K,\ F,\ \tau,\ S_A,\ \text{etc}) \right]$$

$$= f_3 \ (\emptyset,\ K,\ F,\ \tau,\ S_A,\ \text{etc}) \qquad (25)$$

where f_3 is an explicit function.

or

$$f_4 \ (\beta,\ \emptyset,\ K,\ F,\ \tau,\ S_A,\ \text{etc}) = 0 \qquad (26)$$

where f_4 is an implicit function.

Also, it has been shown by previous workers(17)(19)(20) that

$$\tau = f_5 (F, \phi) \quad \text{where } f_5 \text{ is a function} \qquad (27)$$

and

$$F = f_6 (\phi) \quad \text{where } f_6 \text{ is a function} \qquad (28)$$

During this investigation, no attempt was made to collect data on internal surface area, and tortuosity by a means(19) independent of the formation resistivity factor. Therefore, equation 26 was reduced to

$$f_7 (\beta, \phi, K) = 0 \qquad (29)$$

where f_7 is an implicit function relating the variables β, ϕ and K.

A plot of log β versus log $(K)^{0.5}$ indicated relationship as shown in Figure 8. However, a plot of log β versus log ϕ also showed a relationship, as indicated in Figure 9.

In order that the proposed correlation be dimensionally consistent it was observed that the permeability $K(ft^2)$ should appear as $(K)^{0.5}$ in a grouping of ϕ, K, β, and F.

A factor f_s was defined such that

$$f_s = \frac{(9.413 \times 10^{13})^{0.5}}{\beta \cdot (K)^{0.5}} \qquad (30)$$

where the numerator is a conversion factor to convert permeability from ft^2 to mds.

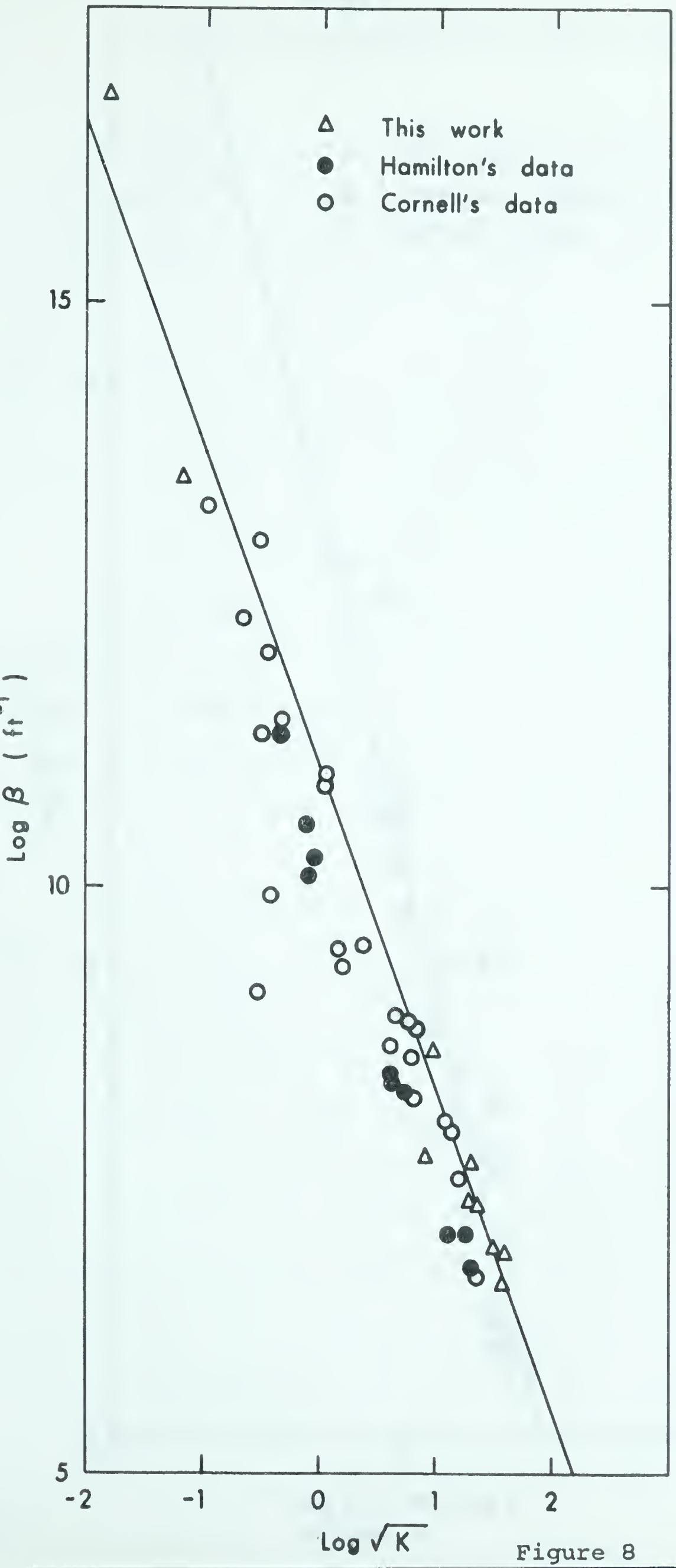
This work
Hamilton's data
Cornell's data
15
10
5
-2
-1
0
1
2
Log β (ft⁻¹)
log √K

Figure 8

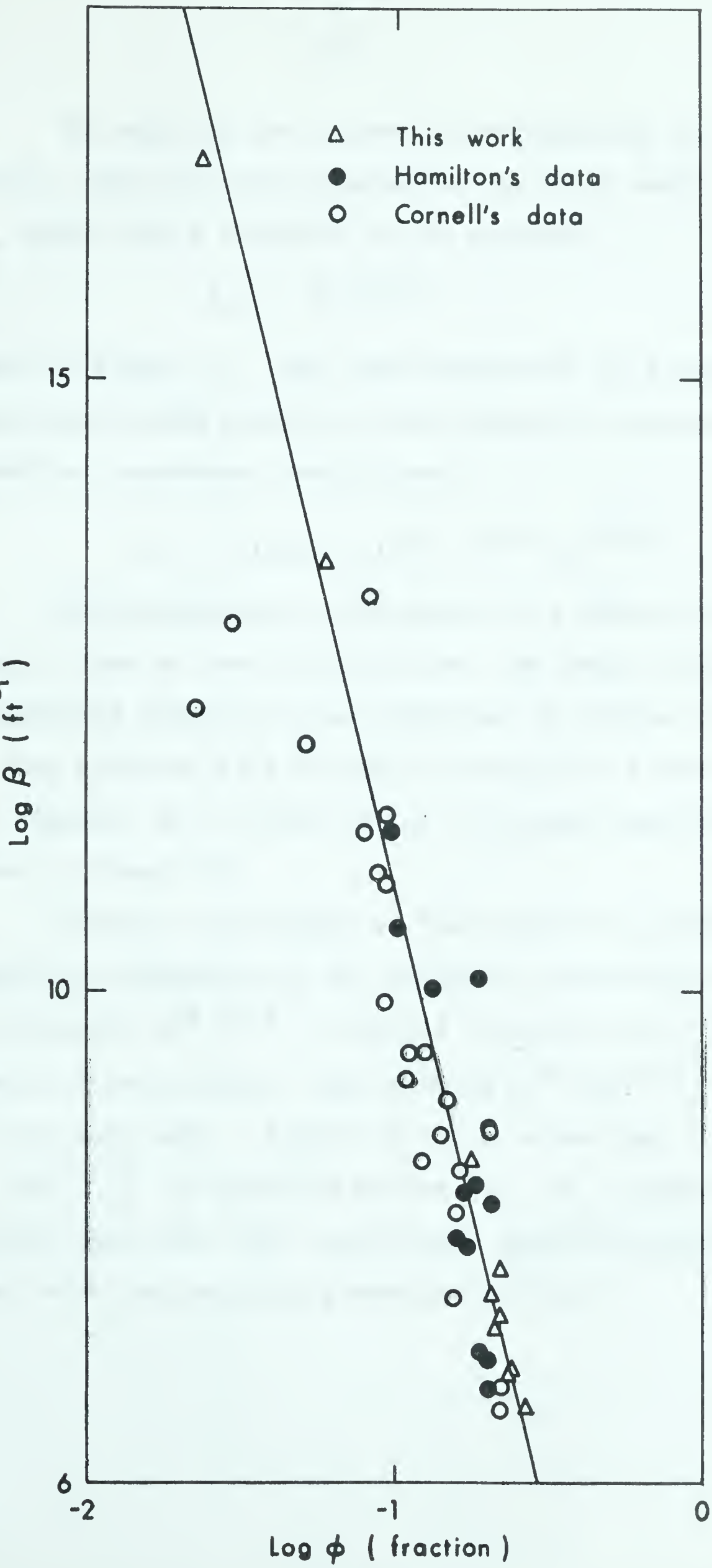
This work
Hamilton's data
Cornell's data
15
10
6
-2
-1
0
Log β (ft⁻¹)
Log ϕ (fraction)

Figure 9

By applying the method of averages(28) to Cornell's, Hamilton's and the data obtained during this study, a plot of log f_s versus log ϕ resulted in the equation

$$f_s = 60\ \phi^{5.07} \tag{31}$$

as shown in Figure 11. The substitution of this value for f_s into equation (30) results in the following expression for the inertial resistance coefficient.

$$\beta = (1.617 \times 10^5)\ K^{-0.5}\ \phi^{-5.07} \tag{32}$$

This expression is proposed as a general correlation. Although it can be used in this form, the same correlation may be represented graphically as indicated in Figure 12. In the event that equation (32) is used to calculate β, the rounding of the exponent of ϕ, from 5.07 to 5.0 seems quite permissable as shown in Figure 13.

Further improvement in the proposed correlation was attempted by incorporating the formation resistivity factor in the grouping $(\phi^5\ K^{0.5})$. Several groupings with different indices of F were tried. The grouping $\left[\phi^5 \cdot (KF)^{0.5}\right]$ appeared to fit the data best. A plot of log β versus log $\left[\phi^5.\ (KF)^{0.5}\right]$ is shown in Figure 14. It is important to mention here that this correlation shows less scatter than any other correlation presented so far.

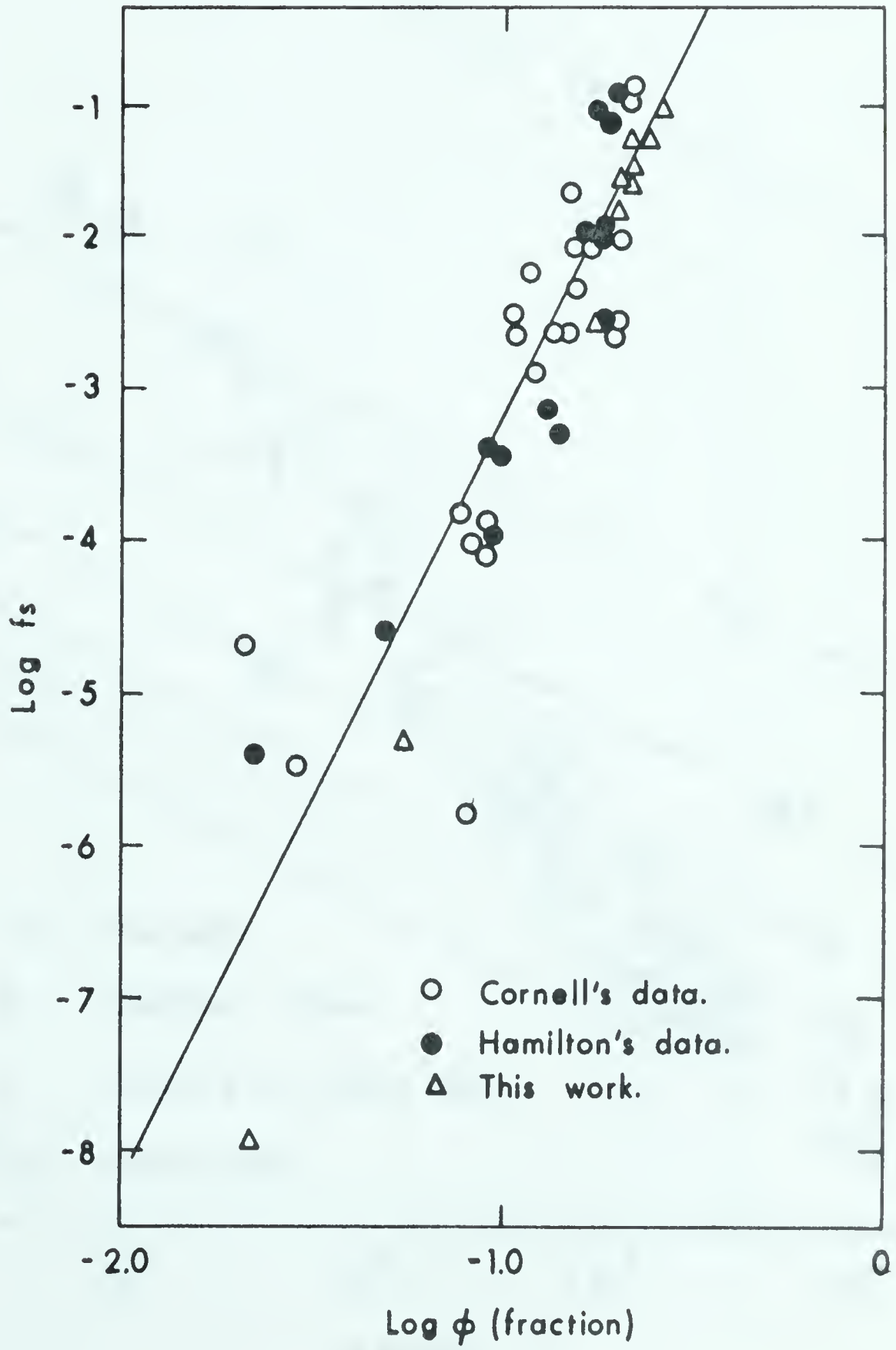
-1
-2
-3
-4
-5
-6
-7
-8
Log fs
-2.0
-1.0
0
Log ϕ (fraction)
Cornell's data.
Hamilton's data.
This work.

Figure 11

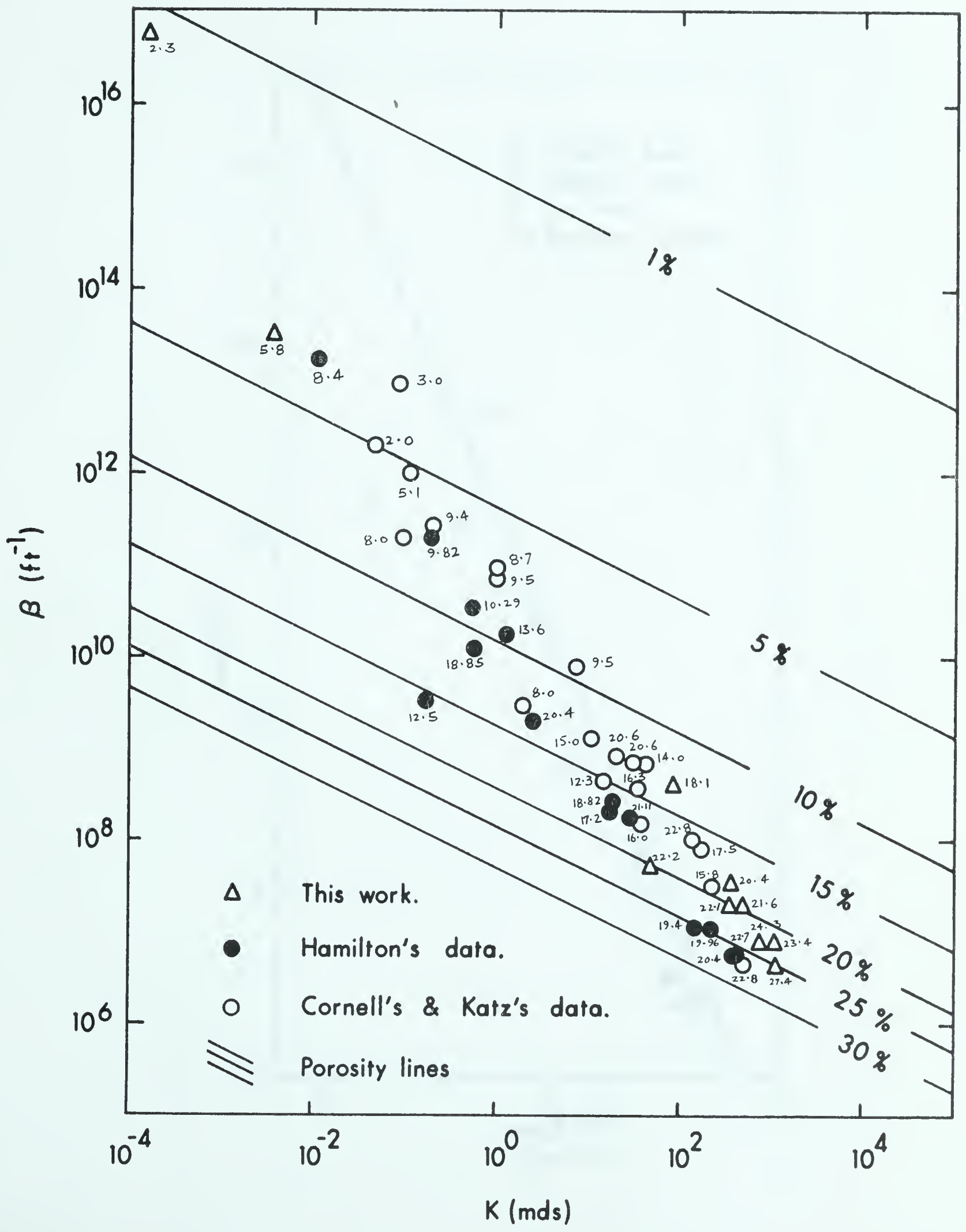

Figure 12. Correlation of Intertial Resistance Coefficient (β) with permeability (K) and porosity (ø)

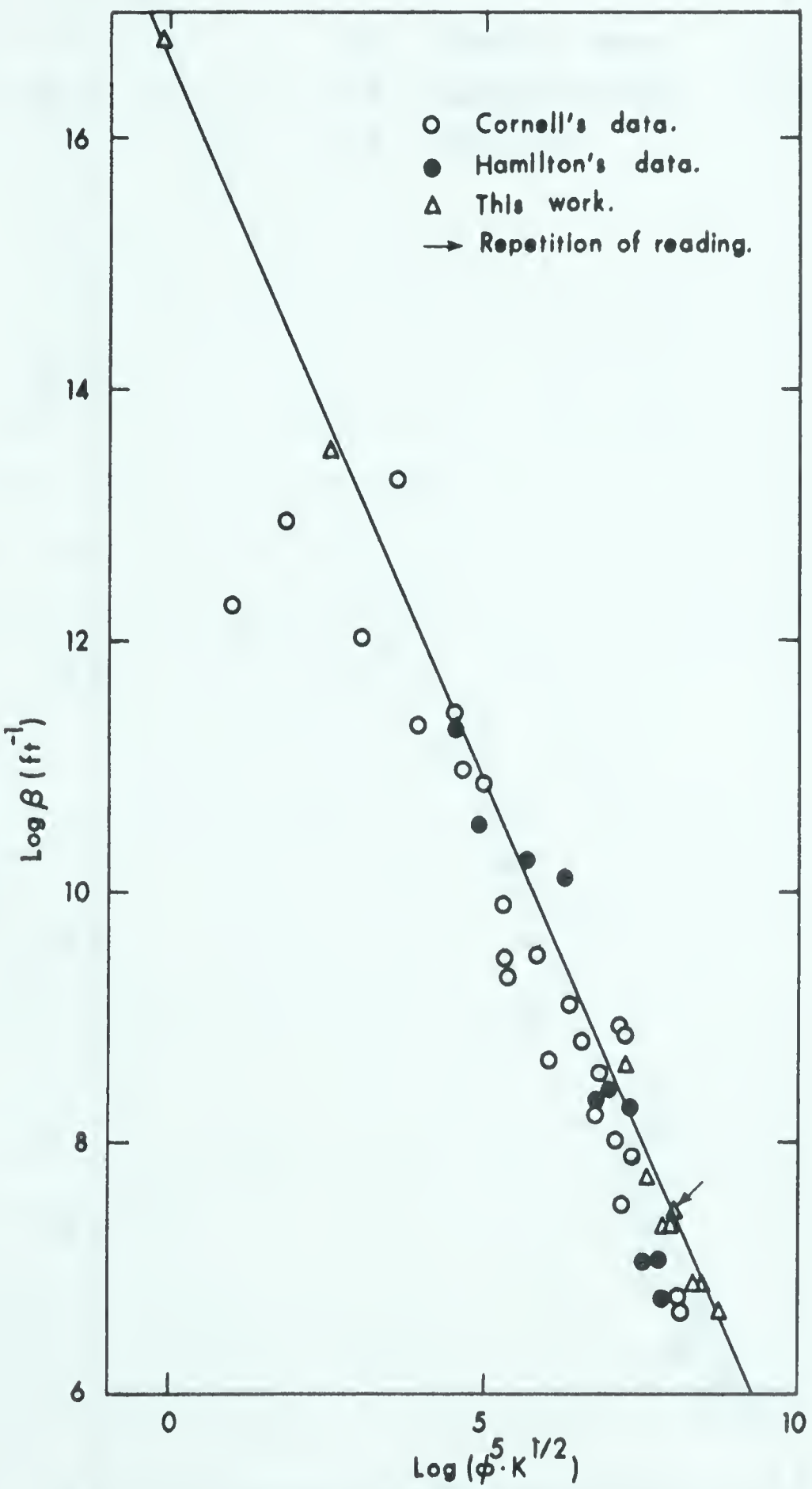
Cornell's data.
Hamilton's data.
This work.
Repetition of reading.
16
14
12
10
8
6
0
5
10
Log β (ft⁻¹)
Log (φ^5 · K^1/2)

Figure 13

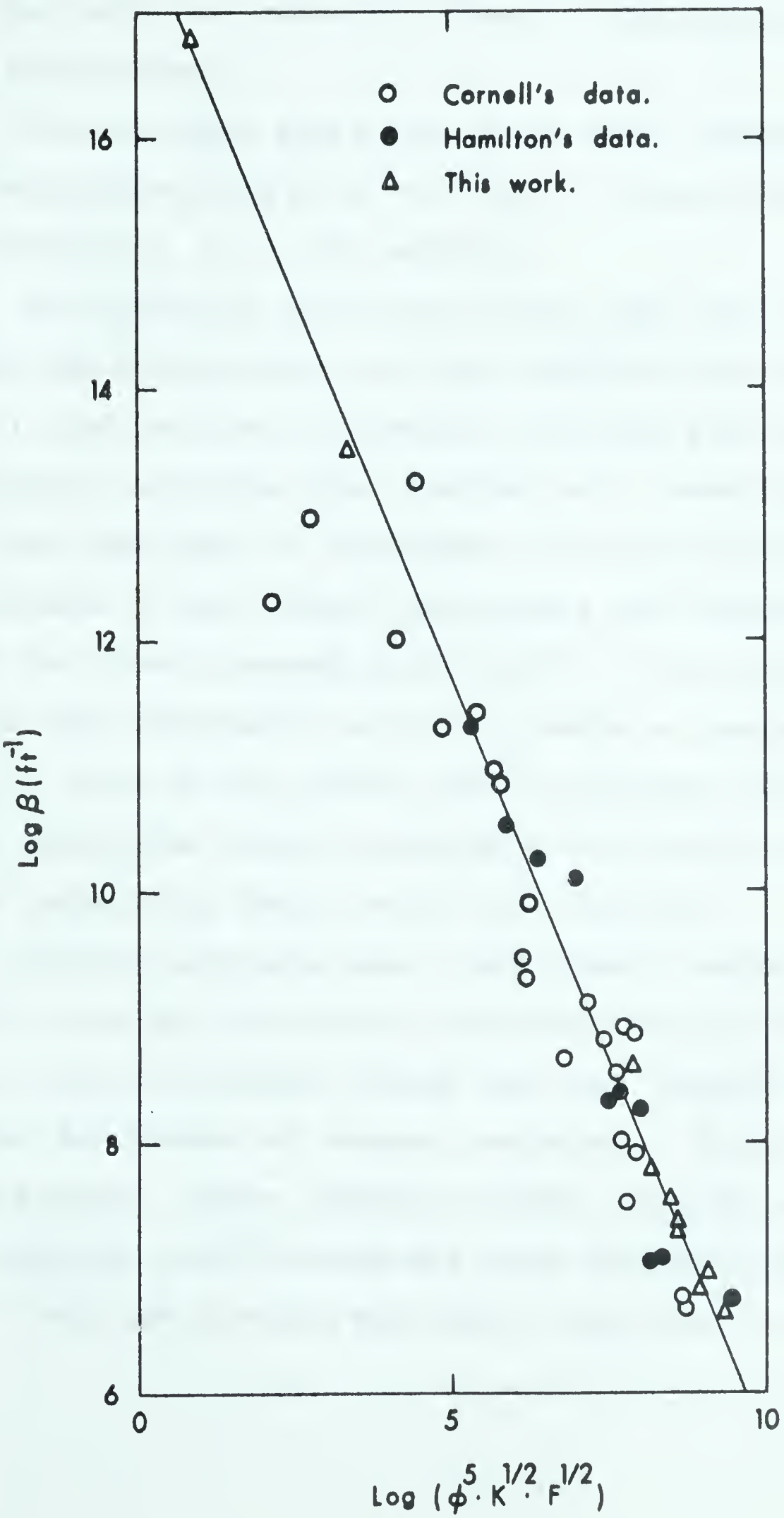
Cornell's data.
Hamilton's data.
This work.
16
14
12
10
8
6
0
5
10
Log β (ft⁻¹)
Log (φ^5 · K^1/2 · F^1/2)

Figure 14

A plot of log f_s vs log F was also attempted but it showed a much wider scatter than the plot of log f_s vs log ϕ. The latter was therefore chosen in developing the proposed correlations.

Several other plots were drawn which indicated the interrelationships among β, ϕ, K, F and τ. Some of these are shown in Figures 7, 8, 9, 10a and 10b.

The formation resistivity factor data were obtained using both the two-electrode and the four-electrode methods. Dunlap(25) reported that the contact resistances may develop at the current electrodes due to either poor connections between the core end areas and the electrodes, or low core saturations. The development of the contact resistances was checked by employing the check proposed by Dunlap(25). The electrical resistance data obtained on all twenty cores is summarized in Table 3. Data on the contact check resistance shows that there was negligible contact resistance and therefore the formation resistivity factor values are reliable.

Several materials were tried to make contact between the core and the current electrodes so as to allow passage of electric current through the core, without any appreciable development of contact resistance. Brine saturated kleenex, sponge, Chamois leather, felt pad and drilling mud were tried but none was found satisfactory. Finally, a felt pad threaded with thin silver wire to form a

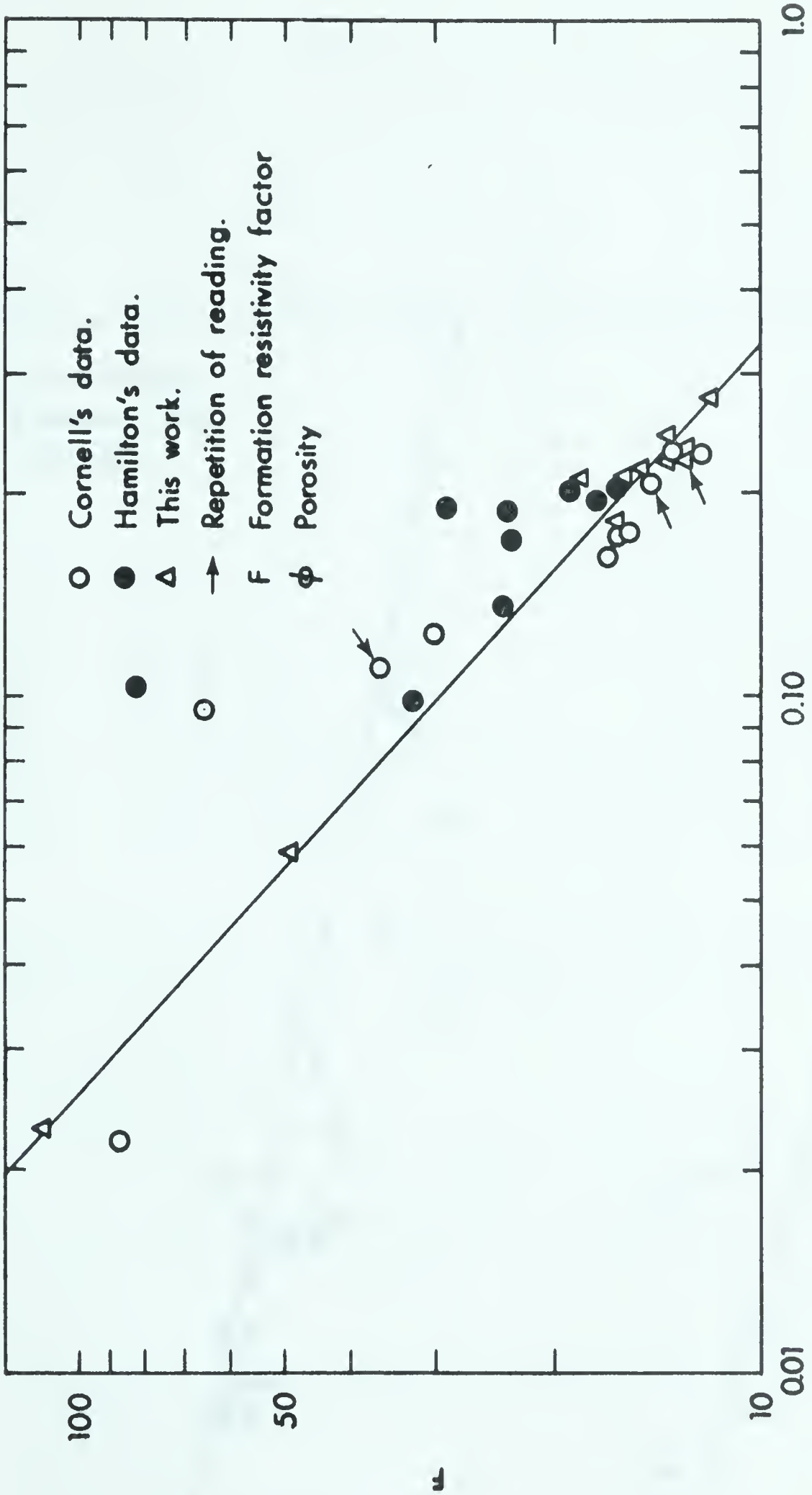
O Cornell's data.
● Hamilton's data.
Δ This work.
→ Repetition of reading.
F Formation resistivity factor
φ Porosity
100
50
10
F
0
0.10
1.0
0.01
φ, (fraction)

Figure 7

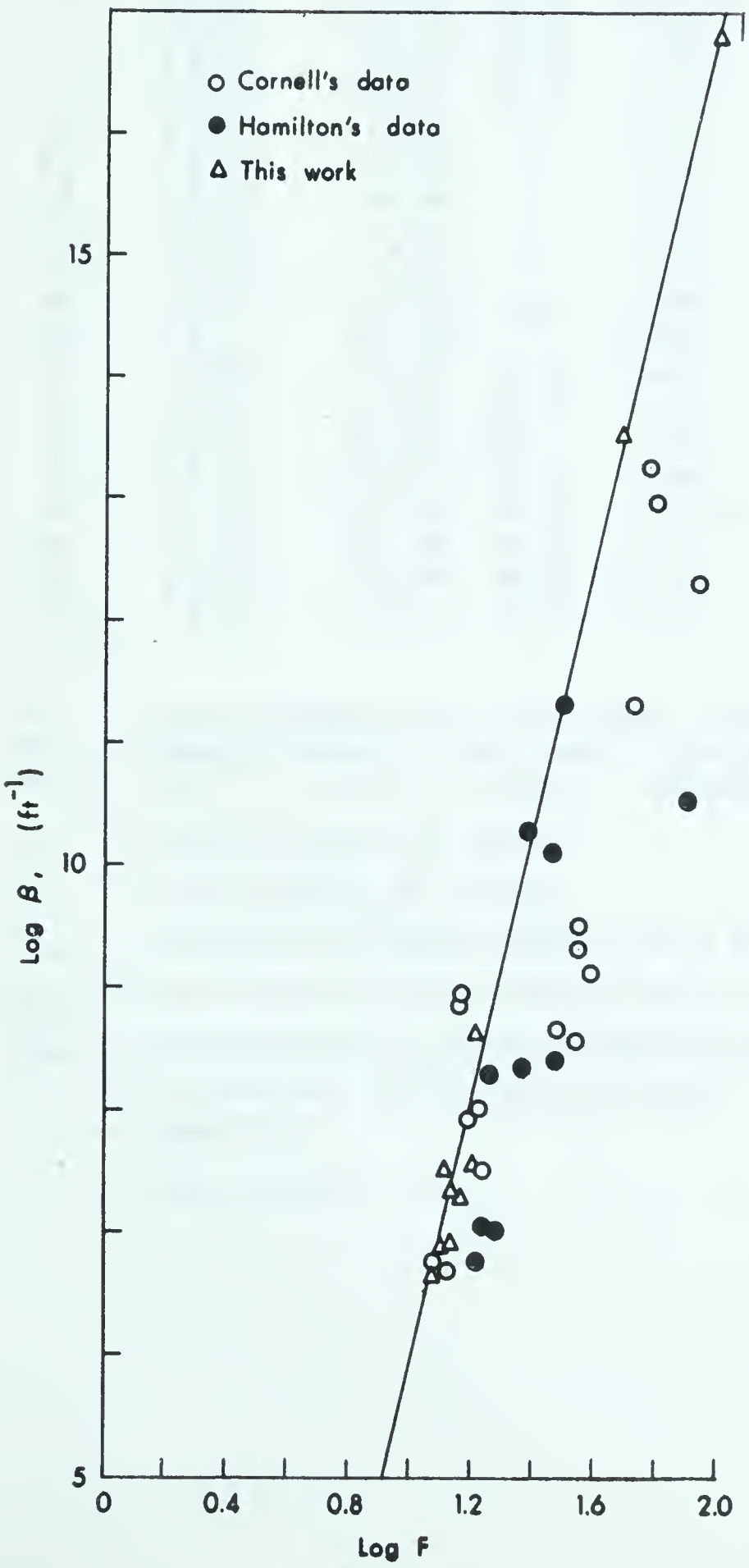

Figure 10a

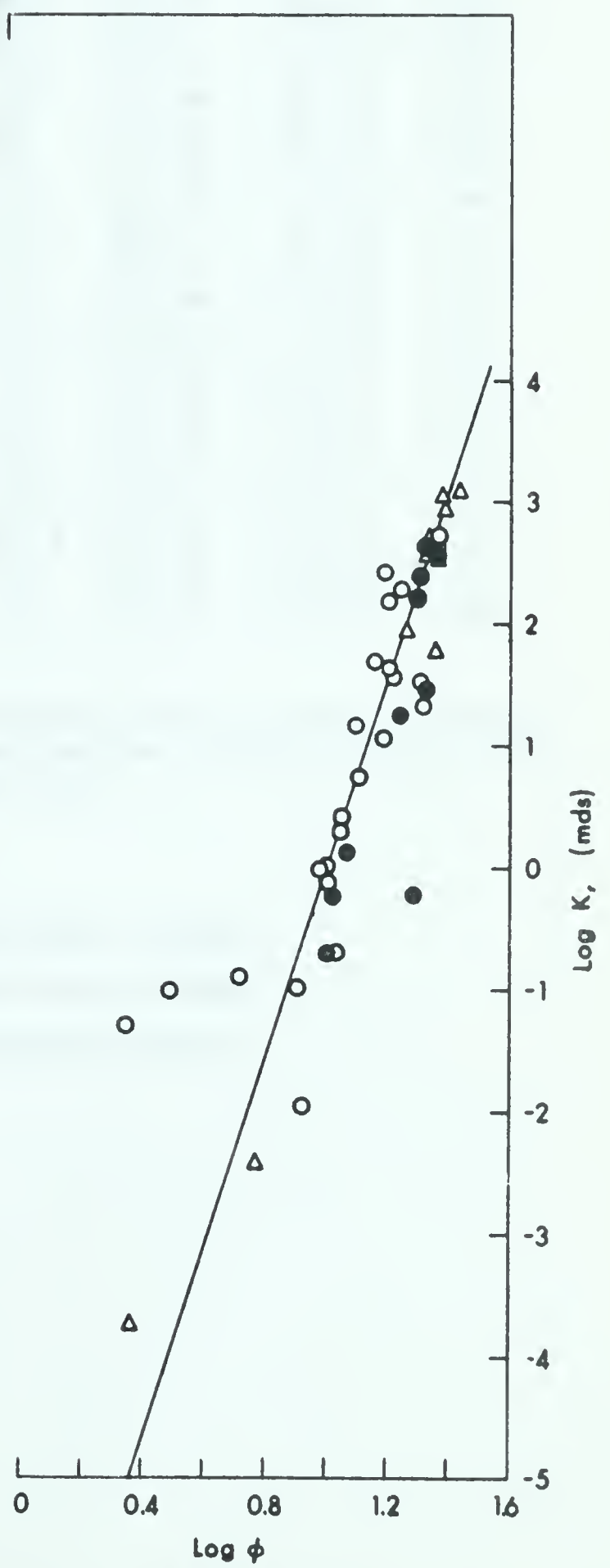

Figure 10b

Table 3

Formation Resistivity Factor and Tortuosity Data

Core No.	ρ_b ohms-cm	R_b ohms**	R_{c4} ohms	R_{c2} ohms	R_{cc} ohms	F	Ø %	τ ***
3	13.53	10.15	80.3	300	150	29.56	18.82	2.36
4	13.53	9.96	62.3	181.5	90.5	18.23	21.11	1.96
5	13.53	10.00	78.8	230	117	23.0	17.16	1.99
7	13.53	10.23	81.3	243.5	123	23.81	13.60	1.80
8	13.53	10.09	47.2	175	86	17.34	19.39	1.83
10	13.53	9.50	*	181	90	19.05	19.96	1.95
11	13.53	8.82	*	145	73	16.44	20.39	1.83
12	13.53	9.30	*	300	145	32.30	9.82	1.78
13	13.53	9.65	*	790	392	82.0	10.28	2.90
14	13.53	9.73	*	283	143	29.07	18.85	2.34
4X	13.53	10.50	45.0	135	65	12.79	22.18	1.68
20	14.1	10.73	*	1200	587.5	111.83	2.30	1.60
22	13.53	10.48	49.0	142	72	13.55	24.33	1.82
24	13.53	10.69	45.9	170	84.5	15.91	20.91	1.82
31	14.1	10.93	160	530	262	48.47	5.84	1.68
38	13.53	10.67	37.9	136	68.0	12.72	23.36	1.72
45	13.53	10.55	39.0	157.5	78.2	14.92	21.55	1.79
46	13.53	10.58	50.8	171	82.5	16.16	18.10	1.71
53	13.53	10.69	40.5	145	72	13.57	22.06	1.73
61	13.53	10.81	33.8	127	64	11.75	27.43	1.80

* Core dimensions such that the probes could not make contact.
** Resistance of the same (congruent)volume of brine solution.
*** $(\tau)^2 = F\emptyset = Le/L$ Reference (5)

ρ_b = resistivity of brine
R_b = resistance of brine
R_{c4} = resistance measurement by 4 electrode method.
R_{c2} = resistance measurement by 2 electrode method.
R_{cc} = resistance of core contact resistance check.
F = formation resistivity factor
Ø = porosity
τ = tortuosity

continuous mesh on both sides, and saturated with brine,was found to be the most suitable of all the techniques proposed so far.

Cornell(14) obtained data on formation resistivity factor by employing an apparatus in which the core sample was placed vertically between two platinum electrodes. During this investigation it was found that the vertical position increased the drainage of brine from the core and thus affected the resistance measurements. Also Cornell(14) did not incorporate any check for detecting the presence of contact check resistance. These two points may account for the scatter observed in Figures 7 and 10a showing the data obtained by Cornell(14), Hamilton(7) and the author.

There is some disagreement over the quantitative relationship between the tortuosity and the formation resistivity factor. Cornell(14), Street(27) and Wyllie and Spangler(17) have suggested different models thus resulting in different expressions.

In order to compare the tortuosity data, obtained in this study with Cornell's data, a model for tortuosity similar to that suggested by Cornell and Katz(15) was used.

Several plots were tried to correlate the permeability with different powers of tortuosity. A plot of $\log (K)^{0.5}$ versus $\log \tau$ was found to show the least scatter of data.

CONCLUSIONS AND RECOMMENDATIONS

Conclusions

1. A general correlation has been developed relating β to porosity, permeability and the formation resistivity factor. Unlike other correlations, this is dimensionally consistent and is not based on the Kozeny model of porous media.

2. The experimental data indicate that the reservoir parameters, i.e. $\emptyset$, K, F and τ are interrelated.

3. The data on Klinkenberg permeability were checked with the permeability values obtained by evaluating α values. Good agreement was observed.

4. The resistance measurements by the two electrode and the four electrode methods are reliable only if no contact resistance is allowed to develop at the current electrode.

5. A brine saturated felt pad, threaded with thin silver wire so as to form a continuous mesh on both sides, was found more suitable as a contact material between the core and the electrode than any other method reported in the literature.

6. Anomalous Klinkenberg permeability data would be obtained if proper care is not exercized to eliminate the effect of slippage.

Although an improved correlation between the inertial resistance coefficient β and the reservoir rock properties is presented herein, it should not be considered as a terminal attempt. The following recommendations are therefore made for

future work:

1. The investigation of other measurable properties of porous media for their influence on β, K and $\emptyset$ is recommended. Some of those properties are the internal surface area, tortuosity by a means independent of formation resistivity factor, surface roughness, pore size distribution, etc.

2. For obtaining data on permeability of very tight rock samples, it is recommended to further investigate the prospects of using Selas porcelain microfilter discs and candles as a volume measuring device.

3. The effectiveness of applying back pressure to restrict the flow to the viscous region should further be studied. The Klinkenberg permeability data should be obtained on several cores, at constant mean pressures but with different flow rates, in order to determine those flow rates that will have to be achieved, before the assumption that the data points fit the straight line(11) is necessarily true.

4. The problem of finding a suitable contact material to carry the electrical current between the current electrodes and the core should further be examined. To minimize errors the resistance measurement cell should be enclosed in a constant temperature and humidity cabinet.

NOMENCLATURE

A	Cross sectional area of porous sample, square inches
D	Diameter of porous sample, inches
D_E	Effective pore diameter of pore structure, (feet)
F	Electrical resistivity factor
f_s	A factor defined by grouping β and K to develop the proposed general correlation
G, G_s	Mass velocity (pound mass/square foot second)
g_c	Conversion factor (32.17 pounds mass x foot/ pounds force x second squared)
K	Permeability of a porous medium to a fluid, millidarcies or (ft^2)
K_1	Dimensionless geometrical constant in the "laminar" term of flow equation - reference (14)
K_2	Dimensionless geometrical constant in the "turbulence" term of flow equation developed by Cornell - reference (14)
K_a	Apparent permeability, millidarcies
K_∞	Klinkenberg permeability (ft^2)
L	Length of porous sample, inches
L_e	Fictitious average path length through a porous medium (ft)
M	Molecular weight of a gas
P_1	Upstream Pressure, (pounds force/sq.inch) absolute
P_2	Downstream pressure, (pounds force/sq.inch) absolute
P_m, $P_{avg.}$	Mean pressure, (pounds force/sq. inch) absolute
Q, q	Flow rate, cubic feet/hour
Q_c, Q_o	Flow rate @ standard conditions

R	Gas constant (1543 pounds force x cubic feet/ square feet x pound mole x °R)
R_c	Resistance of core, ohm
S_A	Internal surface area of a porous medium, ft^2
T	Absolute temperature, °R
v	Velocity, (feet/second)
x	Length of porous medium
Z	Compressibility factor of a gas
α	Viscous resistance coefficient, (ft^{-2})
β	Inertial resistance coefficient, (ft^{-1})
Δ	Difference
μ	Viscosity of gas (pounds mass/foot second)
ρ	Density of gas, (pounds mass/cubic feet)
ρ_b	Resistivity of brine, ohm -cm
τ	Tortuosity
$\emptyset$	Porosity

BIBLIOGRAPHY

1. Grunberg, L. and Nissan, A.H., The Permeability of Porous Solids to Gases and Liquids, Inst. of Pet. Journal 20 (1943) 236, 194.

2. Dranchuk, P.M., Private Communication, (1963).

3. Forchheimer, Philipp, "Hydraulik", Leipzig and Berlin, Druck und Verlag von B.G. Teubner, 1914, Chapter 15, Sections 116-118.

4. Green, L., Jr. and Duwez, P., Fluid Flow Through Porous Metals, Trans ASME (J. App. Mech) (1951) 18, 39.

5. Cornell, D. and Katz, D.L., Flow of Gases Through Consolidated Porous Media, Ind. Eng. Chem. (1953) 45, 2145.

6. Tek, M.R., Coates, K.H., and Katz, D.L., The Effect of Turbulence on the Flow of Natural Gas Through Porous Reservoirs, Jour. of Pet. Tech. (july 1962) 799.

7. Hamilton, R.J., Master's Thesis, Department of Chemical and Petroleum Engineering, University of Alberta, 1963.

8. Scheidegger, A.E., "The Physics of Flow Through Porous Media", The MacMillan Company, (1960).

9. Hubbert, M. King, Darcy's law and the Field Equation of Flow of Underground Fluids, Trans AIME (1956) 207, 222.

10. Hubbert, M. King, The Theory of Ground Water Motion, Jour. of Geology, 8 (1940) 48, 785.

11. Klinkenberg, K.J., The Permeability of Porous Media to Liquids and Gases, API 1941, 200.

12. Stewart, C.R. and Owens, W.H., A Laboratory Study of Laminar and Turbulent Flow in Heterogeneous Porosity Limestones, Trans. AIME (1958) 213, 121.

13. Houpeurt, A., "On Flow of Gases in Porous Media", (in French and English), Revue d' Institut Francais du Petrole. (1959) 14(11): 1468 - 1497, (12): 1637 - 1684.

14. Cornell, D., Ph.D. Thesis, Department of Chemical Engineering, University of Michigan, Ann Arbor, (1952).

15. Katz, D.L., et al, "Handbook of Natural Gas Engineering" McGraw-Hill, (1959).

16. Archie, G.E., The Electrical Resistivity Log as an Aid in Determining Some Reservoir Characteristics, Trans. AIME (1942).

17. Wyllie, M.R.J., and Spangler, M.B., Application of Electrical Resistivity Measurements to Problems of Fluid Flow in Porous Media, Bull, of the Amer. Assoc. Pet. Geol. (1952), 36, 359.

18. Rose, Walter, and Wyllie, M.R.J., Some Theoretical Considerations Related to the Quantitative Evaluation of the Physical Characteristics of Reservoir Rocks from Electric Log Data, Jour. Petrol. Tech., (1950), Vol. 2, No. 4, p. 105.

19. Winsauer, W.O., et al, Resistivity of Brine-Saturated Sands in Relation to Pore Geometry, Bull, of the Amer. Assoc. of Pet. Geol. (1952), 36, 253.

20. Amyx, J.W., et al, "Petroleum Reservoir Engineering", McGraw-Hill, (1960).

21. Beeson, C.A., The Kobe Porosimeter and the Oil Well Research Porosimeter, Trans. AIME 189 (1950) 313.

22. Greenberg, D.B. and Weger, E., An Investigation of the Viscous and Inertia Coefficients for the Flow of Gases Through Porous Sintered Metals with High Pressure Gradients, Chem. Eng. Sci. (1960) 12, 8.

23. Johnston, T.W. and Taliaferro, D.B., Flow of Air and Natural Gas Through Porous Media, Tech. Paper 592, USBM 1938.

24. Rust, C.F., Electrical Resistivity Measurements on Reservoir Rock Samples by the Two-Electrode and Four-Electrode Methods, Trans. AIME (1952), 195, 217.

25. Dunlap, H.F., Bilhartz, H.L., Shuler, E., and Bailey, C.R., The Relations Between Electrical Resistivity and Brine Saturations in Reservoir Rocks," Trans. AIME, (1949) 186, 259.

26. Helsenrath, J., et al, National Bull. of Std. Circular 584 (1955), 357.

27. Street , N., Tortuositv Concepts, Australian Jour. Chem. (1958), 11, 607.

28. Kenney, J.F., and Keeping, E.S., Mathematics of Statistics Part 1, 3rd edition, D. Van Nostrand Co., Inc., Toronto (1954), Sections 15, 14, p. 279.

APPENDIX I

Table 4

Brine Saturation Data

Core No.	Weight of dry core (gms)	Weight of saturated core (gms)	Weight of brine admitted (gms)	Density of brine (gm/cc)	Volume of brine admitted cc	Pore Volume cc	% Saturation
3	41.4538	45.0173	3.5635	1.0299	3.460	3.593	96.3
4	39.1756	43.1211	3.9455	1.0299	3.831	3.945	97.1
5	40.9280	44.0939	3.1659	1.0299	3.074	3.202	96.0
7	45.2031	47.7521	2.5490	1.0299	2.475	2.605	95
8	40.1338	43.7879	3.6541	1.0299	3.548	3.646	97.3
10	40.6277	44.5042	3.8765	1.0299	3.764	3.825	98.4
11	37.1664	40.7577	3.5913	1.0299	3.487	3.628	96.1
12	45.0628	46.8610	1.7982	1.0299	1.746	1.842	94.8
13	46.1567	48.1094	1.9527	1.0299	1.896	2.002	94.7
14	43.0610	46.7470	3.6860	1.0299	3.579	3.701	96.7
4X	38.2610	42.4352	4.1742	1.0299	4.053	4.17	97.2
20	48.5223	48.9219	0.3996	1.0299	0.388	0.42	92.3
22	37.3703	41.9946	4.6243	1.0299	4.490	4.60	97.6
24	40.7383	45.0144	4.2761	1.0299	4.152	4.28	97.0
31	46.3197	47.3517	1.0320	1.0299	1.002	1.08	92.8
38	38.7568	43.2894	4.5326	1.0299	4.401	4.50	97.8
45	37.9757	41.8924	3.9167	1.0299	3.803	3.90	97.5
46	41.9569	45.6790	3.7221	1.0299	3.614	3.73	96.9
53	39.5116	44.5983	5.0867	1.0299	4.939	5.05	97.8
61	37.8055	43.5544	5.7489	1.0299	5.582	5.69	98.1

Table 5

Viscous Flow Data
Core Number 4X

Run No.	Pressure, psia P_1	P_2	$\frac{1}{P_m}$ $(psia)^{-1}$	$(P_1^2 - P_2^2)$ $(psia)^2$	T_f °R	Q_c SCFH	K (md)
1	14.97	13.465	0.0703	42.88	537.0	0.058	65.2
2	17.41	13.479	0.0648	121.29	536.2	0.158	62.2
3	19.90	13.612	0.0597	210.56	534.0	0.275	62.2
4	22.83	13.516	0.0550	338.39	535.8	0.434	61.4
5	26.42	13.550	0.0500	514.52	535.7	0.669	62.2
6	30.65	13.597	0.0452	754.42	535.7	0.967	61.4
7	36.52	13.684	0.0398	1146.24	535.6	1.446	60.4
8	42.15	14.676	0.0352	1561.24	535.7	1.957	60.0
9	47.45	19.159	0.0300	1884.2	531.2	2.39	60.3
10	53.47	26.685	0.0250	2146.8	531.3	2.689	59.5
11	64.55	35.71	0.0200	2891.4	531.6	3.551	58.4
12	80.29	52.60	0.0151	3679.1	532.9	4.409	57.2
13	118.4	92.21	0.0095	5525.1	533.0	6.380	55.2

Table 6

Visco-Inertial Flow Data
Core Number 4X

Run No.	Pressure, psia P_1	P_2	Q_c SCFH	T_f °R	$\frac{G_s}{\mu} \times 10^2$ (ft^{-1})	$\frac{\Delta P^2}{G_s} \times 10^9$ $\frac{lb_f^2\ sec}{lb_m\ ft^2}$	$T_f \mu Z L \times 10^5$	$\frac{M\ g_c\ \Delta(P^2)}{2\mu L(ZRT)G_s} \times 10^{11}$ (ft^{-2})
1	213.1	22.97	38.32	535.0	124.98	6.252	1.415	23.032
2	188.1	20.39	31.43	536.0	102.59	5.955	1.417	21.899
3	165.0	18.20	25.32	538.0	82.64	5.660	1.422	20.732
4	156.1	17.73	23.41	533.0	76.43	5.487	1.409	20.296
5	116.6	15.37	14.12	532.2	46.15	5.047	1.405	18.711
6	115.5	15.15	13.64	538.0	44.60	5.119	1.420	18.787
7	115.5	15.18	13.50	535.0	44.10	5.171	1.413	19.062
8	103.6	14.800	11.51	532.0	37.62	4.893	1.405	18.150
9	88.5	14.275	8.55	532.0	27.95	4.788	1.405	17.754
10	78.52	13.912	6.94	535.0	22.68	4.603	1.412	16.984
11	58.52	13.716	3.86	535.5	12.63	4.495	1.413	16.577
12	38.55	13.520	1.62	536.0	5.30	4.292	1.414	15.817

Table 7

Viscous Flow Data
Core Number 20

Run No.	Pressure, psia P_1	P_2	$\frac{1}{P_m}$ $(psia)^{-1}$	$P_1^2 - P_2^2$ $(psia)^2$	T_f °R	Q_c SCFH	K (md)
1	260.3	13.307	0.0073	67577	532.2	0.000399	0.000275
2	316.2	13.298	0.0061	99804	532.2	0.000532	0.000249
3	375.1	13.298	0.0052	140522	532.2	0.000715	0.000238
4	437.3	13.301	0.0044	191054	532.2	0.000888	0.000218
5	488.8	13.300	0.004	238749	532.6	0.00105	0.000205
6	586.8	13.300	0.0033	344157	532.7	0.00142	0.000194
7	693.3	13.300	0.0028	480488	532.9	0.00187	0.000184
8	839.3	13.302	0.0024	704251	533.1	0.00250	0.000168
9	985.7	13.304	0.0020	971435	533.3	0.00328	0.000161
10	1122.3	13.309	0.0018	1259394	533.7	0.00403	0.000153
11	1391.9	13.311	0.0014	1937231	534.0	0.00581	0.000144
12	1543.1	13.309	0.0013	2381005	534.1	0.00677	0.000138
13	1659.3	13.307	0.0012	2753119	534.3	0.00779	0.000135

Table 8

Visco-Inertial Flow Data
Core Number 20

Run No.	Pressure, psia P_1	P_2	Q_c SCFH	T_f °R	$\frac{G_s}{\mu} \times 10^{-1}$ (ft^{-1})	$\frac{\Delta P^2}{G_s} \times 10^{15}$ $\frac{lb_f^2 \ sec}{lb_m \ ft^2}$	$T \ \mu ZL \times 10^5$	$\frac{M \ g_c \ \Delta P^2}{2\mu L(ZRT)G_s} \times 10^{17}$ (ft^{-2})
1	289.3	13.296	0.000521	532.1	1.68	0.862	1.373	3.270
2	316.2	13.298	0.000532	532.2	1.72	1.009	1.374	3.824
3	375.1	13.298	0.000715	532.2	2.31	1.057	1.375	4.004
4	437.3	13.301	0.000888	532.2	2.86	1.157	1.376	4.378
5	488.8	13.300	0.00105	532.6	3.51	1.178	1.379	4.449
6	586.8	13.300	0.00142	532.7	4.56	1.303	1.381	4.918
7	693.3	13.300	0.0187	532.9	5.99	1.381	1.384	5.198
8	839.3	13.302	0.00250	533.1	7.98	1.514	1.389	5.681
9	1122.3	13.309	0.00403	533.7	12.75	1.680	1.403	6.240
10	1391.9	13.311	0.00581	534.0	18.21	1.793	1.415	6.601
11	1543.1	13.309	0.00677	533.1	21.10	1.891	1.420	6.939
12	1659.3	13.307	0.00779	533.3	24.17	1.9	1.427	6.939

Table 9

Viscous Flow Data
Core Number 22

Run No.	Pressure, psia P_1	P_2	$\frac{1}{P_m}$ $(psia)^{-1}$	$P_1^2 - P_2^2$ $(psia)^2$	T_f °R	Q_c SCFH	K (md)
1	16.45	13.809	0.0661	79.81	532.3	1.716	1020
2	18.38	14.582	0.0607	125.30	532.3	2.673	1012
3	19.29	15.393	0.0577	135.08	532.7	2.749	966.5
4	19.83	16.342	0.0553	126.05	532.8	2.593	977.2
5	21.68	18.214	0.0501	138.45	533.0	2.807	964
6	23.87	20.314	0.0453	157.21	533.1	3.134	948
7	26.59	23.608	0.0398	149.58	533.3	2.982	940
8	30.58	27.274	0.0346	191.45	533.5	3.696	918.5
9	34.82	31.93	0.0300	193.05	533.7	3.697	912
10	41.63	38.73	0.0249	233.53	533.8	4.329	883
11	50.87	48.50	0.0201	236.0	534.0	4.305	870
12	67.54	65.42	0.0150	281.87	534.0	4.683	793
13	101.27	98.42	0.0100	569.09	537.9	8.65	732
14	101.25	98.70	0.0100	509.87	534.0	7.31	692

Table 10

Visco-Inertial Flow Data
Core Number 22

Run No.	Pressure, psia P_1	P_2	Q_c SCFH	T_f °R	$\frac{G_s}{\mu} \times 10^2$ (ft^{-1})	$\frac{\Delta P^2}{G_s} \times 10^8$ $\frac{lb_f\ sec}{lb_m\ ft^2}$	$T_f \mu Z L \times 10^5$	$\frac{M\ g_c\ \Delta P^2}{2\mu L(ZRT)G_s} \times 10^{10}$ (ft^{-2})
1	142.07	98.374	74.245	533.5	235.104	7.960	1.450	28.592
2	104.90	86.700	52.988	534.1	167.979	6.521	1.457	23.418
3	89.53	37.281	53.55	534.3	169.810	6.794	1.451	24.390
4	59.50	24.10	31.07	536.2	98.663	5.229	1.454	18.731
5	63.53	21.91	26.83	536.0	85.122	4.894	1.455	17.522
6	48.53	20.195	23.95	536.0	76.032	4.475	1.455	16.027
7	43.53	18.60	20.02	536.0	63.574	4.248	1.454	15.216
8	39.61	17.47	17.30	534.6	54.967	4.015	1.450	14.439
9	35.96	17.37	14.07	534.6	44.710	3.862	1.450	13.876
10	33.01	16.46	12.245	534.0	38.911	3.659	1.448	13.161
11	29.69	15.637	10.13	533.6	32.197	3.453	1.447	12.434
12	27.00	15.038	8.415	534.8	26.749	3.267	1.450	11.738
13	23.79	14.425	6.40	535.0	20.346	3.062	1.450	10.999
14	22.49	14.260	5.608	534.6	17.832	2.972	1.449	10.687
15	20.95	14.073	4.665	534.0	14.834	2.834	1.447	10.201
16	19.98	13.965	4.016	534.0	12.771	2.783	1.447	10.019
17	19.19	13.882	3.528	534.0	11.219	2.723	1.447	9.802

Table 11

Viscous Flow Rate
Core Number 24

Run No.	Pressure, psia P_1	P_2	$\frac{1}{P_m}$ $(psia)^{-1}$	$P_1^2 - P_2^2$ $(psia)^2$	T_f °R	Q_c SCFH	K (md)
1	19.66	13.660	0.0600	199.96	537.3	2.067	505
2	21.50	14.777	0.0551	243.72	533.0	2.477	492.7
3	23.43	16.398	0.0502	279.88	533.3	2.772	480.7
4	25.54	18.464	0.0455	311.47	533.5	3.011	469.3
5	28.55	21.405	0.0400	356.76	533.8	3.360	457.6
6	31.64	25.481	0.0350	351.94	534.1	3.308	456.9
7	36.60	29.995	0.0300	439.71	534.3	3.965	438.5
8	52.60	47.27	0.0200	532.67	534.9	4.500	412.1
9	101.25	98.35	0.0100	578.84	535.6	4.601	388.5

Table 12

Visco-Inertial Flow Data
Core Number 24

Run No.	Pressure, psia P_1	P_2	Q_c (SCFH)	T_f °R	$\frac{G_s}{\mu} \times 10^2$ (ft^{-1})	$\frac{\Delta P^2}{G_s} \times 10^8$ $\frac{lb_f\ sec}{lb_m\ ft^2}$	$T_f \mu Z L \times 10^5$	$\frac{M\ g_c\ \Delta P^2}{2\mu L(ZRT)G_s} \times 10^{11}$ (ft^{-2})
1	13.94	13.508	0.135	534	0.43	4.751	1.490	1.687
2	14.88	13.533	0.419	533	1.32	5.015	1.487	1.784
3	15.64	13.566	0.660	532.8	2.08	5.107	1.487	1.817
4	16.81	13.608	1.026	532.0	3.23	5.289	1.485	1.885
5	18.74	13.566	1.640	532.3	5.17	5.462	1.486	1.945
6	20.80	13.836	2.240	534.3	7.06	5.965	1.491	2.116
7	24.69	14.020	3.517	534.5	11.08	6.688	1.492	2.372
8	29.72	14.310	5.166	535.5	16.27	7.273	1.495	2.574
9	32.28	14.52	6.125	535.7	19.29	7.493	1.495	2.651
10	34.86	14.74	7.00	535.7	22.05	7.909	1.495	2.799
11	37.35	14.98	7.81	535.9	24.60	8.310	1.497	2.938
12	40.65	15.35	9.05	536.0	28.49	8.688	1.497	3.071
13	43.65	15.66	10.00	536.4	31.48	9.188	1.498	3.245
14	53.66	17.09	13.54	535.7	46.63	10.580	1.496	3.742
15	67.61	19.69	18.63	534.7	58.64	12.446	1.493	4.410
16	93.60	23.50	29.42	534.8	92.49	15.450	1.495	5.467
17	112.4	27.80	36.77	534.8	115.52	17.819	1.496	6.302
18	142.6	36.10	48.69	534.5	152.96	21.592	1.495	7.642
19	180.3	44.12	64.50	532.7	202.48	26.193	1.490	9.301

Table 13

Viscous Flow Data
Core Number 31

Run No.	Pressure, psia P_1	P_2	$\frac{1}{P_m}$ $(psia)^{-1}$	$P_1^2 - P_2^2$ $(psia)^2$	T_f °R	Q_c SCFD	K (md)
1	83.5	13.441	0.0206	6972	533.8	0.00121	0.00826
2	103.4	13.441	0.0171	10519	534.2	0.00164	0.00744
3	116.5	13.483	0.0154	13387	534.9	0.00195	0.00697
4	129.4	13.441	0.0140	16574	534.4	0.00234	0.00674
5	163.6	13.489	0.0113	26570	535	0.00353	0.00636
6	199.5	13.504	0.0094	39620	535.1	0.00476	0.00576
7	223.5	13.528	0.0084	49782	531.0	0.00588	0.00562
8	273.5	13.533	0.0070	74634	531.5	0.00832	0.00532
9	317.6	13.550	0.0059	100708	531.9	0.0109	0.00517
10	419.6	13.554	0.0046	175859	532.5	0.0178	0.00483
11	535.5	13.554	0.0036	286619	533.0	0.0267	0.00448
12	533.5	13.545	0.0037	284471	534.0	0.0261	0.00443
13	603.5	13.547	0.0032	364064	534.3	0.0323	0.00428
14	703.5	13.492	0.0028	494688	537.9	0.0409	0.00403
15	808.5	13.497	0.0024	653438	537.9	0.0524	0.00392
16	929.5	13.504	0.0021	863821	538.0	0.0664	0.00377
17	1065.5	13.507	0.0019	1135133	538.0	0.843	0.00366
18	1213.5	13.495	0.0016	1472364	533.7	0.111	0.00369
19	1382.4	13.511	0.0014	1910944	533.7	0.139	0.00357
20	1573.4	13.531	0.0013	2475521	533.9	0.171	0.00344

Table 14

Viscous-Inertial Flow Data
Core Number 31

Run No.	Pressure, psia P_1	P_2	Q_c SCFH	T_f °R	$\frac{G_s}{\mu}$ (ft^{-1})	$\frac{\Delta P^2}{G_s} \times 10^{13}$ $\frac{lb_f\ sec}{lb_m\ ft^2}$	$T_f \mu Z L \times 10^5$	$\frac{M\ g_c\ \Delta P^2}{2\mu LZRTG_s} \times 10^{16}$ (ft^{-2})
1	83.5	13.441	0.001207	533.8	0.39	0.3118	1.430	1.136
2	103.4	13.441	0.001638	534.2	0.53	3.466	1.431	1.262
3	116.5	13.483	0.001951	534.9	0.63	3.704	1.433	1.346
4	129.4	13.441	0.002335	534.4	0.75	4.571	1.432	1.663
5	163.6	13.489	0.00353	535.0	1.14	4.060	1.434	1.475
6	199.5	13.504	0.004758	535.1	1.53	4.495	1.436	1.631
7	223.5	13.528	0.005876	531.0	1.88	4.573	1.425	1.672
8	273.5	13.533	0.008324	531.5	2.67	4.840	1.428	1.766
9	419.6	13.554	0.01782	532.5	5.70	5.327	1.433	1.936
10	535.5	13.554	0.02668	533.0	8.51	5.799	1.437	2.106
11	533.5	13.545	0.02614	534.0	8.34	5.874	1.440	2.125
12	603.5	13.547	0.03227	534.3	10.28	6.09	1.443	2.198
13	703.5	13.492	0.04088	537.9	12.99	6.532	1.456	2.337
14	808.5	13.497	0.05242	537.9	16.62	6.729	1.459	2.403
15	929.5	13.504	0.06637	538.0	20.97	7.025	1.463	2.502
16	1065.5	13.507	0.08429	538.0	26.51	7.269	1.470	2.577
17	1213.5	13.495	0.1105	533.7	34.56	7.192	1.466	2.557
18	1382.4	13.511	0.1386	533.7	43.11	7.442	1.473	2.631
19	1573.4	13.531	0.1710	533.9	52.72	7.814	1.485	2.742

Table 15

Viscous Flow Data
Core Number 38

Run No.	Pressure, psia P_1	P_2	$\frac{1}{P_m}$ $(psia)^{-1}$	$P_1^2 - P_2^2$ $(psia)^2$	T_f °R	Q_c SCFH	K (md)
1	16.94	14.072	0.0645	89.1	536.9	2.272	1244
2	19.06	14.700	0.0592	147.2	536.8	3.717	1230
3	19.32	15.308	0.0578	138.9	536.5	3.486	1220
4	20.51	16.316	0.0543	154.5	536.5	3.840	1210
5	22.01	18.015	0.0500	159.9	536.5	3.801	1190
6	24.01	21.124	0.0443	130.1	536.5	3.109	1165
7	26.13	23.74	0.040	119.0	536.5	2.879	1178
8	29.96	27.45	0.035	143.8	533.3	3.411	1149
9	34.34	32.50	0.030	122.8	533.5	2.943	1161
10	41.06	39.03	0.025	162.5	533.7	3.706	1106
11	135.45	134.36	0.0074	294.0	535.0	6.174	1027

Table 16

Visco-Inertial Data
Core Number 38

Run No.	Pressure, psia P_1	P_2	Q_c SCFH	T_f °R	$\frac{G_s}{\mu} \times 10^2$ (ft^{-1})	$\frac{\Delta P^2}{G_s} \times 10^8$ $\frac{lb_f \times sec}{lb_m \times ft^2}$	$T_f \mu Z L \times 10^5$	$\frac{M g_c \Delta P^2}{2\mu LZRTG_s} \times 10^{10}$ (ft^{-2})
1	18.75	13.968	3.74	536.8	11.88	2.294	1.481	8.067
2	21.25	14.295	5.43	534.9	17.27	2.495	1.476	8.806
3	23.25	14.655	6.97	534.7	22.17	2.567	1.476	9.064
4	26.18	15.263	8.99	535.0	28.59	2.764	1.477	9.753
5	27.07	15.620	10.20	535.3	32.44	2.619	1.477	9.235
6	30.67	16.530	11.97	535.3	38.05	3.060	1.477	10.788
7	35.84	18.140	15.42	535.4	49.00	3.394	1.478	11.960
8	41.63	19.270	20.20	535.5	64.18	3.703	1.479	13.045
9	52.53	22.82	28.40	536.0	90.22	4.360	1.480	15.347
10	68.53	29.70	40.30	536.2	127.97	5.205	1.481	18.306
11	84.23	37.46	51.60	536.3	163.65	5.986	1.483	21.029
12	105.52	48.40	68.66	536.2	217.72	7.040	1.483	24.734
13	138.52	66.72	95.60	535.4	302.94	8.523	1.481	29.980

Table 17

Viscous Flow Data
Core Number 45

Run No.	Pressure, psia P_1	P_2	$\frac{1}{P_m}$ $(psia)^{-1}$	$P_1^2 - P_2^2$ $(psia)^2$	T_f °R	Q_c SCFH	K (md)
1	14.77	13.438	0.0709	37.7	535.1	0.518	661.5
2	16.54	13.570	0.0664	89.4	535.1	1.118	601.1
3	16.48	13.979	0.0657	76.1	535.2	1.010	638.9
4	18.52	14.709	0.0602	126.5	535.2	1.608	611.7
5	20.25	15.407	0.0561	172.6	535.7	2.138	596.5
6	22.44	17.594	0.0500	194.1	535.7	2.350	582.9
7	23.64	20.768	0.0499	127.5	535.7	1.629	570.0
8	25.60	23.810	0.0403	88.6	535.8	1.261	558.0
9	29.15	27.476	0.0352	94.5	535.8	1.384	545.0
10	33.91	32.505	0.0300	93.5	536.0	1.354	535.1
11	40.74	39.448	0.0249	103.8	536.0	1.525	518.0
12	52.11	47.252	0.0201	482.9	537.5	5.023	505.2
13	101.24	98.292	0.0100	588.6	538.3	5.794	479.5

Table 18

Visco-Inertial Flow Data
Core Number 45

Run No.	Pressure, psia P_1	P_2	Q_c SCFH	T_f °R	$\frac{G_s}{\mu} \times 10^2$ (ft^{-1})	$\frac{\Delta P^2}{G_s} \times 10^8$ $\frac{lb_f \times sec}{lb_m \times ft^2}$	$T_f \mu Z L \times 10^5$	$\frac{M g_c \Delta P^2}{2\mu LZRTG_s} \times 10^{11}$ (ft^{-2})
1	25.43	14.042	4.89	537.0	15.65	4.979	1.458	1.779
2	29.61	14.437	6.63	537.0	21.21	6.532	1.458	2.334
3	48.41	17.448	13.98	538.2	44.71	7.905	1.461	2.818
4	57.59	18.243	19.07	538.0	60.94	8.484	1.462	3.024
5	73.39	21.543	26.66	538.0	84.86	10.041	1.463	3.577
6	89.39	25.993	34.62	539.0	110.55	11.454	1.465	4.073
7	99.89	28.933	39.51	539.0	126.19	12.540	1.465	4.459
8	115.4	33.293	47.28	538.8	150.97	13.993	1.465	4.977
9	137.95	41.275	59.58	538.8	190.15	15.762	1.465	5.604
10	161.9	48.418	71.69	538.6	228.63	18.049	1.465	6.417
11	189.4	58.328	86.49	538.0	275.66	20.358	1.465	7.242
12	210.9	66.100	97.87	537.5	311.75	22.216	1.464	7.908

Table 19

Viscous Flow Data
Core Number 46

Run No.	Pressure, psia P_1	P_2	$\frac{1}{P_m}$ $(psia)^{-1}$	$P_1^2 - P_2^2$ $(psia)^2$	T_f °R	Q_c SCFH	K (md)
1	15.09	13.53	0.070	44.7	540.1	0.085	93.3
2	16.88	13.53	0.066	105.1	540.0	0.195	94.0
3	19.32	14.06	0.060	175.4	540.0	0.333	93.0
4	19.88	14.51	0.058	184.6	531.3	0.354	92.5
5	21.41	14.84	0.055	238.2	532.0	0.455	92.0
6	22.37	18.15	0.049	170.8	532.2	0.322	91.0
7	24.77	20.08	0.045	210.4	532.3	0.390	89.5
8	27.10	22.63	0.040	222.3	532.3	0.411	89.3
9	30.20	26.38	0.035	216.3	532.7	0.395	88.2
10	34.63	31.89	0.030	182.2	533.0	0.329	87.4
11	41.44	38.76	0.025	214.6	533.3	0.386	87.0
12	51.49	48.31	0.020	317.4	533.7	0.551	84.1
13	100.8	98.6	0.010	446.5	533.8	0.660	71.7

Table 20

Visco-Inertial Flow Data
Core Number 46

Run No.	Pressure, psia P_1	P_2	Q_c SCFH	T_f °R	$\frac{G_s}{\mu} \times 10^2$ (ft^{-1})	$\frac{\Delta P^2}{G_s} \times 10^9$ $\frac{lb_f\ sec}{lb_m\ sec}$	$T_f \mu Z L \times 10^5$	$\frac{M g_c \Delta P^2}{2\mu L Z R T G_s} \times 10^{12}$ (ft^{-2})
1	15.17	13.385	0.097	535.0	0.304	2.922	1.479	1.029
2	17.34	13.393	0.226	535.0	0.712	2.986	1.479	1.052
3	19.62	13.387	0.383	534.7	1.205	2.976	1.478	1.049
4	22.26	13.391	0.561	534.7	1.766	3.125	1.479	1.101
5	25.86	13.412	0.815	534.7	2.565	3.325	1.479	1.174
6	29.08	13.432	1.073	534.7	3.376	3.438	1.479	1.211
7	48.86	13.632	2.781	534.7	8.744	4.185	1.479	1.474
8	62.27	13.867	4.330	534.7	13.616	4.707	1.480	1.657
9	81.6	14.322	6.515	534.0	20.481	5.477	1.478	1.944
10	110.8	15.365	9.950	534.4	31.257	6.701	1.480	2.359
11	139.3	16.892	13.412	535.3	42.096	7.886	1.483	2.771
12	173.3	19.260	17.950	535.3	56.317	9.173	1.484	3.221

Table 21

Viscous Flow Data*
Core Number 53

Run No.	Pressure, psia P_1	P_2	$\frac{1}{P_m}$ $(psia)^{-1}$	$P_1^2 - P_2^2$ $(psia)^2$	T_f °R	Q_c SCFH	K (md)
1	14.56	13.509	0.0713	29.50	537.0	0.282	469.0
2	17.90	13.639	0.0634	134.50	537.8	1.263	460.9
3	21.50	13.884	0.0565	269.66	538.0	2.472	450.0
4	23.77	18.248	0.0476	231.88	537.0	2.082	440.6
5	29.03	22.07	0.0391	355.42	538.3	3.090	425.1
6	37.63	30.60	0.0293	479.66	536.1	4.037	411.0
7	52.25	46.45	0.0203	572.48	536.0	4.708	402.1
8	101.45	98.3	0.0100	623.30	536.5	4.814	375.0
9	136.50	133.5	0.0074	810.00	536.7	5.985	360.0

* The data were obtained by applying back pressure.

Table 22

Anomalous Data for Klinkenberg Permeability*
Core Number 53

Run No.	Pressure, psia P_1	P_2	$\frac{1}{P_m}$ $(psia)^{-1}$	$P_1^2 - P_2^2$ $(psia)^2$	T_f °R	Q_c SCFH	K (md)
1	15.36	13.314	0.0698	59.0	535.5	0.54	447
2	18.87	13.402	0.0620	176.0	535.5	1.59	439.5
3	22.33	13.544	0.0558	314.1	535.3	2.71	418.5
4	26.14	13.670	0.0503	498.0	533.5	4.09	397.3
5	30.13	14.025	0.0453	712.0	535.3	5.50	374.0
6	34.37	14.34	0.0411	974.0	533.8	7.10	352.0
7	51.25	16.828	0.0294	2351	535.3	13.90	288.0
8	88.05	23.79	0.0197	7213	538.3	30.60	206.0
9	114.8	31.33	0.0136	12216	535.2	43.50	172.5
10	140.3	39.34	0.0112	18450	534.8	56.16	148.0
11	167.3	48.25	0.0093	25670	534.3	64.8	122.6

* Calculated without back pressure.

Table 23

Visco-Inertial Flow Data
Core Number 53

Run No.	Pressure, psia P_1	P_2	Q_c SCFH	T_f °R	$\frac{G_s}{\mu} \times 10^2$ (ft^{-1})	$\frac{\Delta P^2}{G_s} \times 10^8$ $\frac{lb_f\ sec}{lb_m\ ft^2}$	$T_f \mu Z L \times 10^5$	$\frac{Mg_c\ \Delta P^2}{2\mu LZRTG_s} \times 10^{11}$ (ft^{-2})
1	17.91	13.64	1.263	537.8	4.002	5.830	1.492	2.036
2	17.94	13.58	1.211	537.5	3.838	6.207	1.491	2.169
3	21.51	13.89	2.461	538.0	7.798	5.934	1.492	2.071
4	28.99	14.72	5.08	538.0	16.095	6.720	1.493	2.346
5	33.73	15.50	6.874	538.1	21.755	7.153	1.495	2.493
6	37.63	30.60	4.04	534.1	12.786	7.778	1.483	2.732
7	40.88	15.23	9.615	535.3	30.55	8.244	1.481	2.901
8	43.67	35.88	5.08	538.7	16.075	6.679	1.496	2.326
9	51.25	16.83	13.90	535.3	44.152	9.259	1.481	3.257
10	52.25	46.45	5.18	536.0	16.394	7.248	1.488	2.537
11	61.4	18.64	20.22	538.3	64.209	11.050	1.490	3.864
12	70.03	63.26	6.825	536.3	21.562	7.238	1.490	2.530
13	88.05	23.79	30.6	538.3	97.135	12.904	1.481	4.538
14	102.40	97.36	7.082	536.7	22.363	7.791	1.481	2.741
15	114.75	31.33	43.5	535.2	138.057	15.37	1.481	5.406
16	133.41	128.09	9.608	537.0	30.328	7.925	1.493	2.766
17	139.34	39.34	56.16	534.8	170.809	17.414	1.481	6.124

Table 24

Viscous Flow Data
Core Number 61

Run No.	Pressure, psia P_1	P_2	$\frac{1}{P_m}$ $(psia)^{-1}$	$P_1^2 - P_2^2$ $(psia)^2$	T_f °R	Q_c SCFH	K (md)
1	19.24	14.46	0.0594	161.2	538.2	4.545	1395
2	21.04	15.01	0.0555	217.1	538.2	5.896	1344
3	23.16	16.89	0.0999	251.3	538.2	6.656	1311
4	25.37	19.40	0.0447	267.5	538.2	7.010	1298
5	27.60	22.38	0.0400	260.9	538.2	6.837	1297
6	31.50	25.70	0.0350	331.9	538.2	8.349	1245
7	35.93	31.03	0.0299	327.8	538.2	8.258	1248
8	41.84	37.92	0.0251	313.2	538.2	7.906	1250
9	51.98	47.86	0.0200	511.3	538.2	10.177	1226
10	100.85	98.81	0.0100	409.3	538.2	9.284	1126

Table 25

Visco-Inertial Flow Data
Core Number 61

Run No.	Pressure, psia P_1	P_2	Q_c SCFH	T_f °R	$\frac{G_s}{\mu} \times 10^2$ (ft^{-1})	$\frac{\Delta P^2}{G_s} \times 10^8$ $\frac{lb_f\ sec}{lb_m\ ft^2}$	$T_f \mu Z L \times 10^5$	$\frac{Mg_c\ \Delta P^2}{2\mu LZRTG_s} \times 10^{10}$ (ft^{-2})
1	25.59	15.37	9.85	533.5	31.12	2.348	1.501	8.147
2	36.95	29.60	11.03	532.9	34.60	2.450	1.510	8.455
3	43.32	36.92	10.72	537.6	33.71	2.649	1.519	9.084
4	47.81	22.78	28.3	539.2	89.09	3.497	1.522	11.968
5	52.58	47.28	10.6	531.0	33.23	2.759	1.505	9.549
6	54.12	46.45	14.53	537.5	45.71	2.932	1.518	10.062
7	71.01	63.95	17.42	537.4	54.73	3.063	1.520	10.501
8	77.24	38.98	54.5	536.0	171.33	4.508	1.515	15.511
9	105.08	102.60	10.33	534.0	32.34	2.755	1.515	9.474
10	139.35	87.75	101.4	536.0	318.10	6.389	1.517	21.936
11	203.51	195.21	44.46	539.2	138.99	4.114	1.524	14.063

APPENDIX II

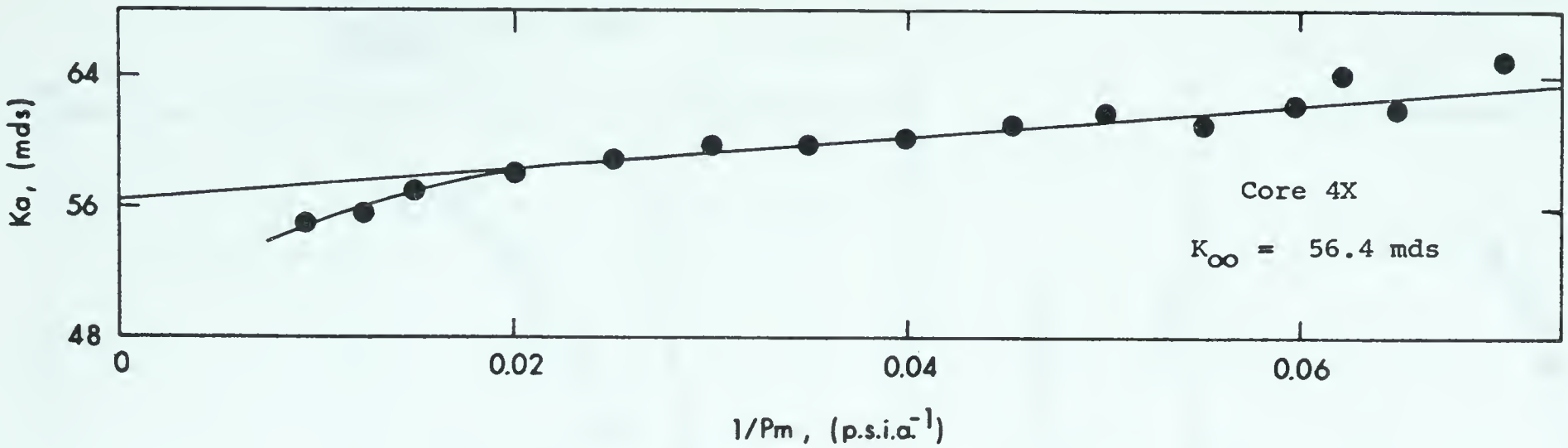

Figure 1-A. Klinkenberg Permeability Plot

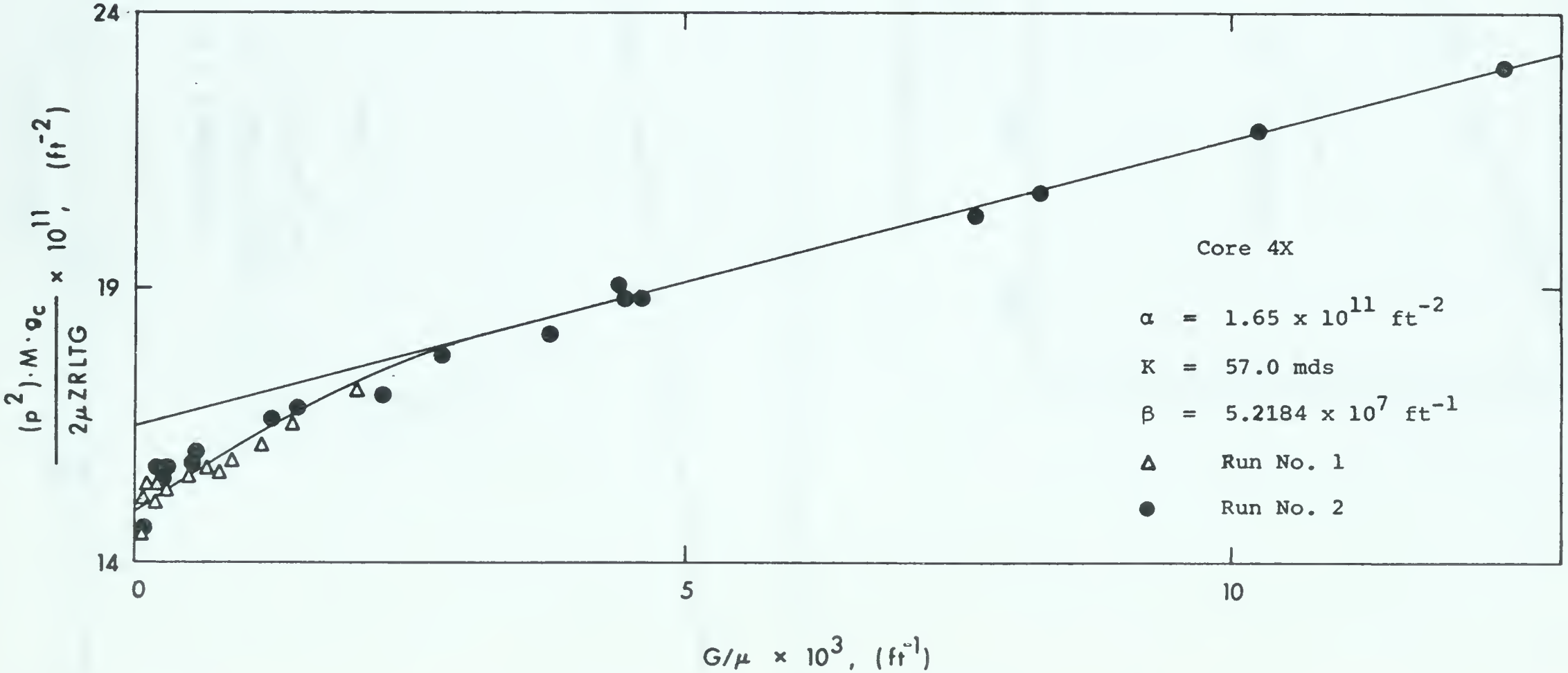

Figure 2-A. Flow Data Plot to Calculate α and β

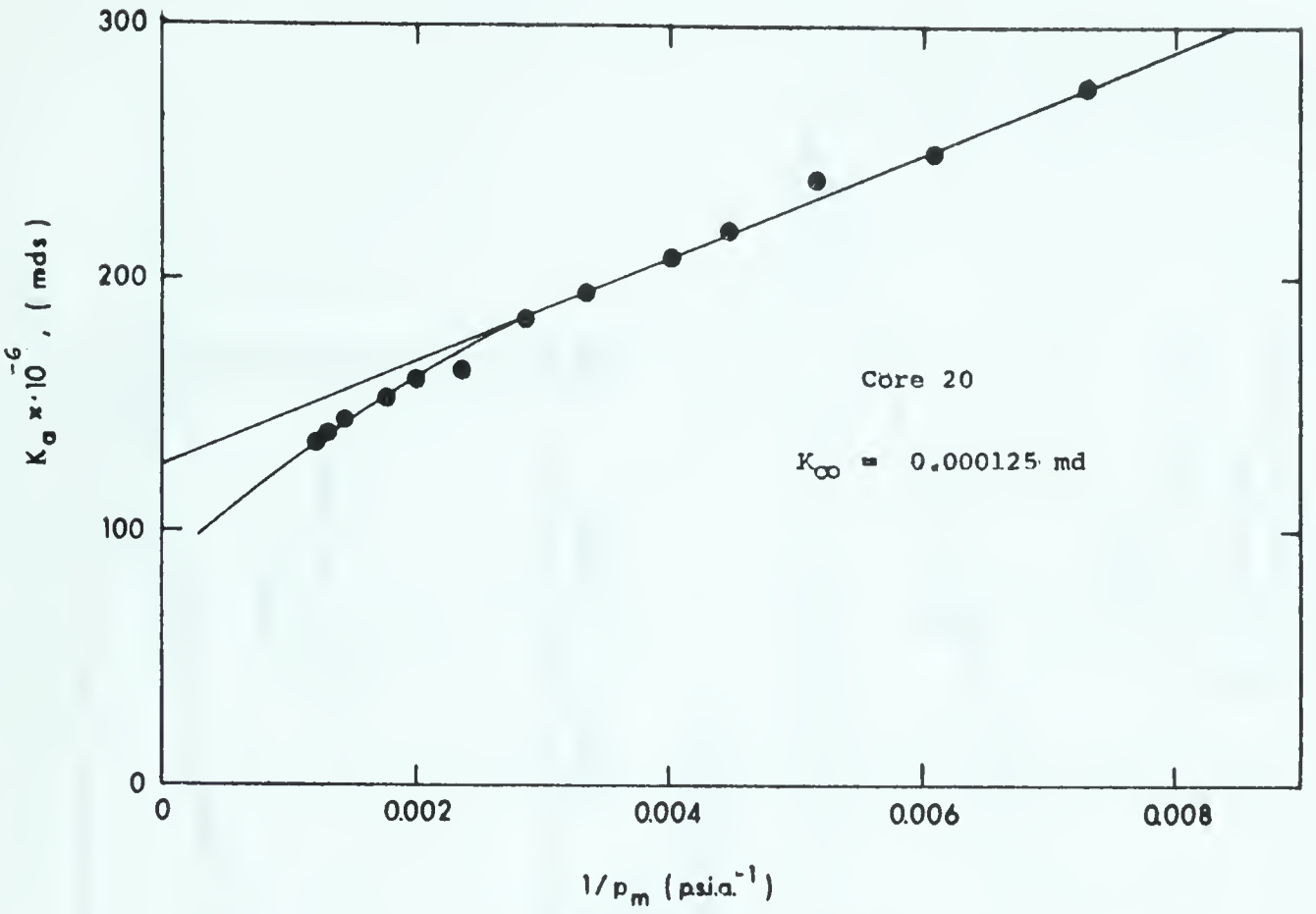

Figure 3-A. Klinkenberg Permeability Plot

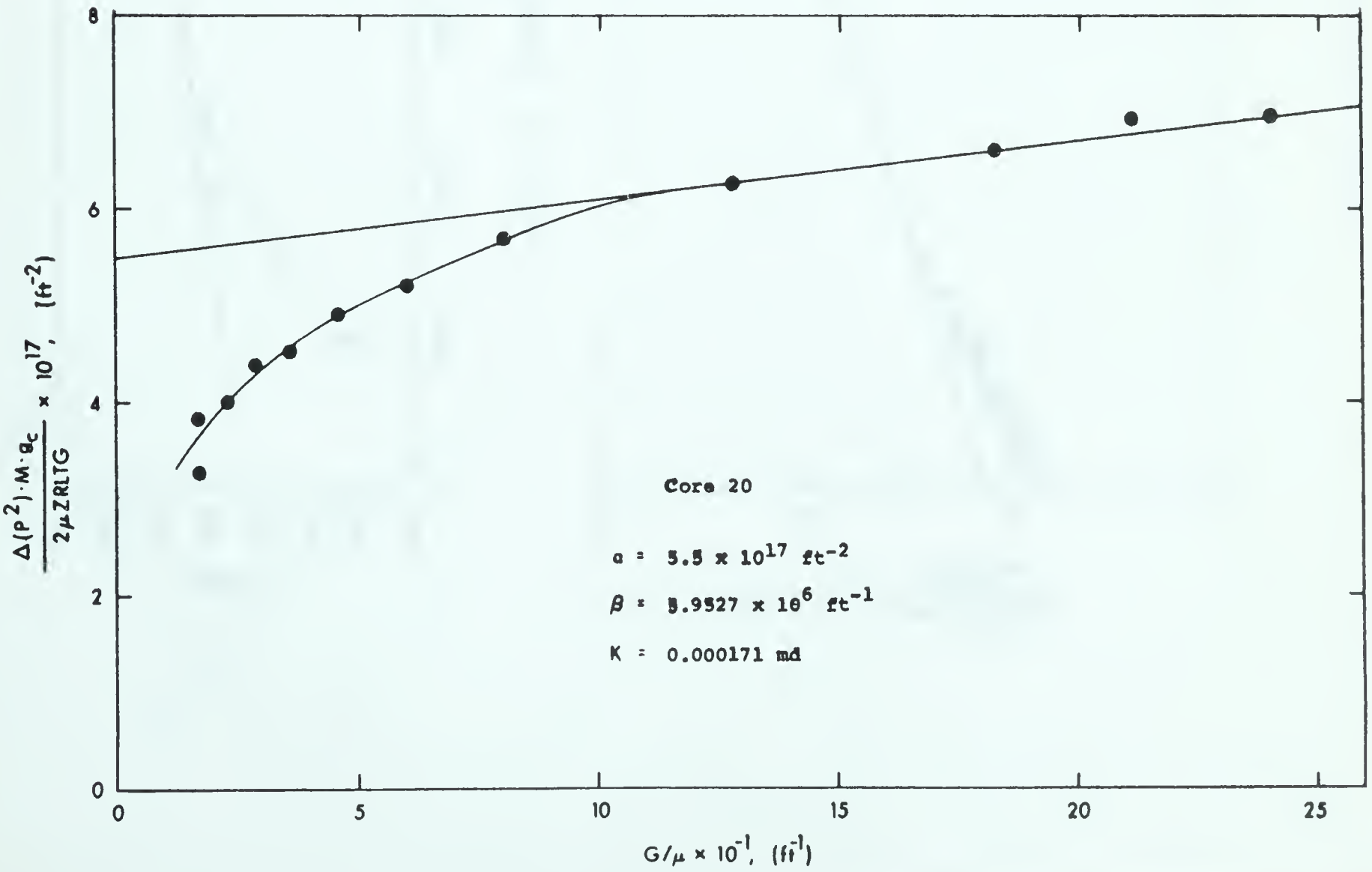

Fig. 4-A. Flow Data Plot to Calculate α and β

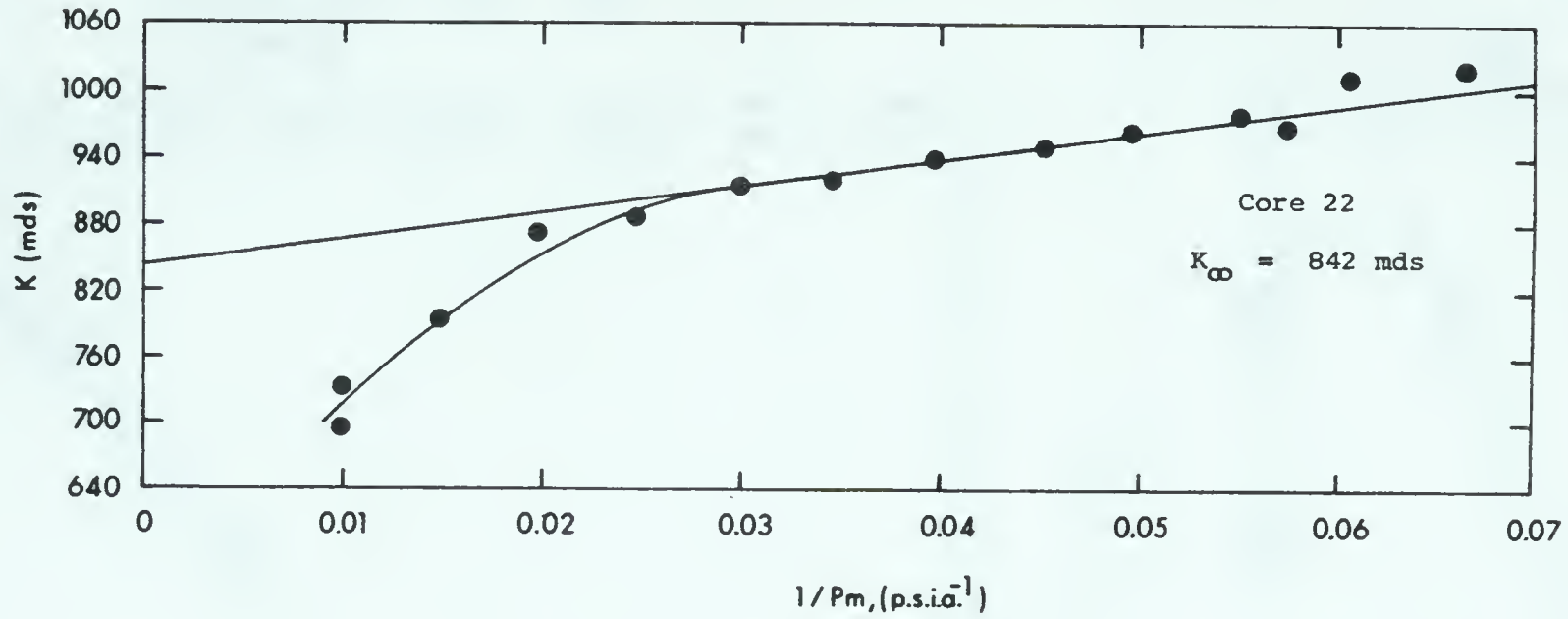

Figure 5-A. Klinkenberg Permeability Plot

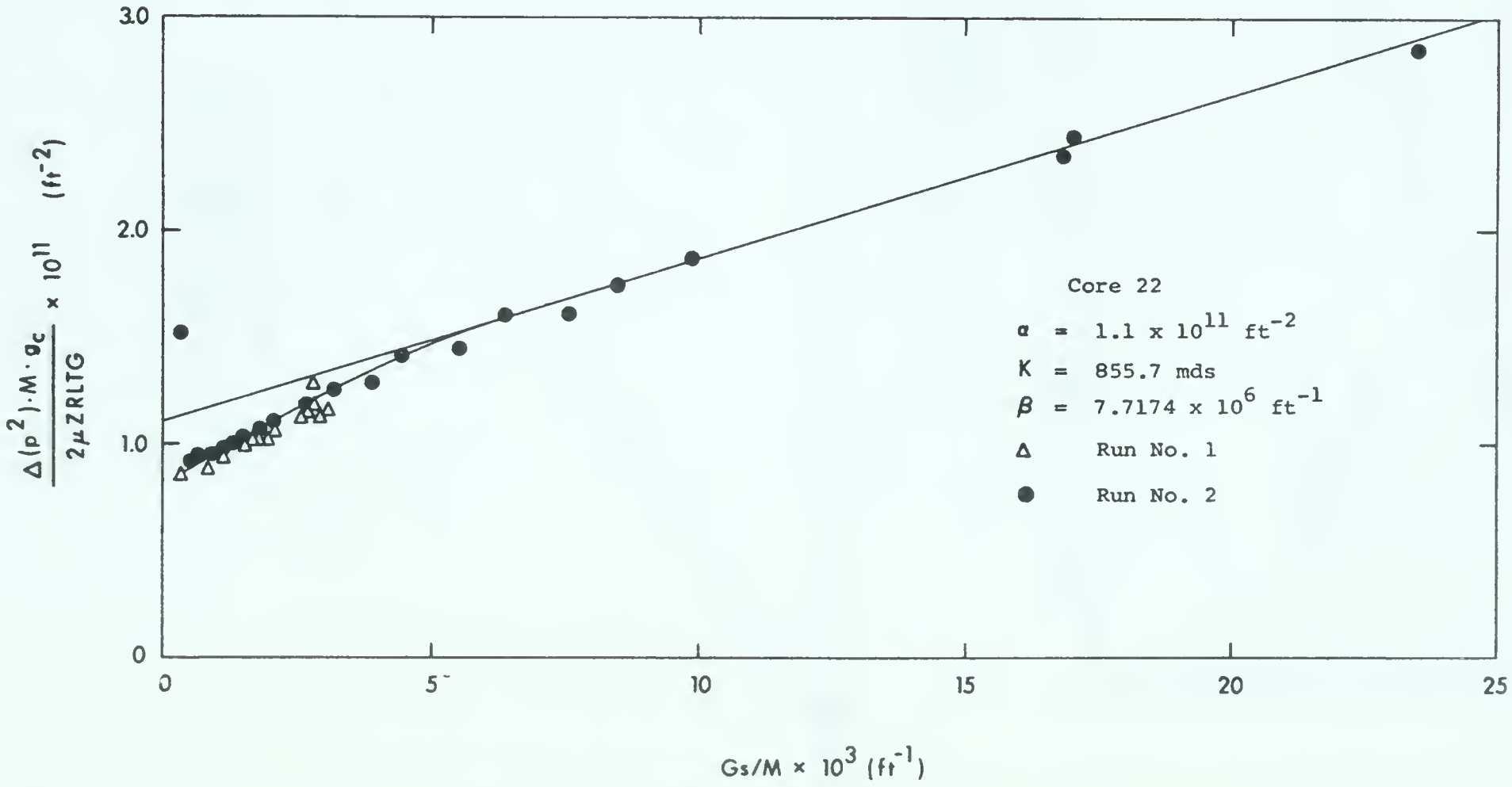

Figure 6-A. Flow Data Plot to Calculate α and β

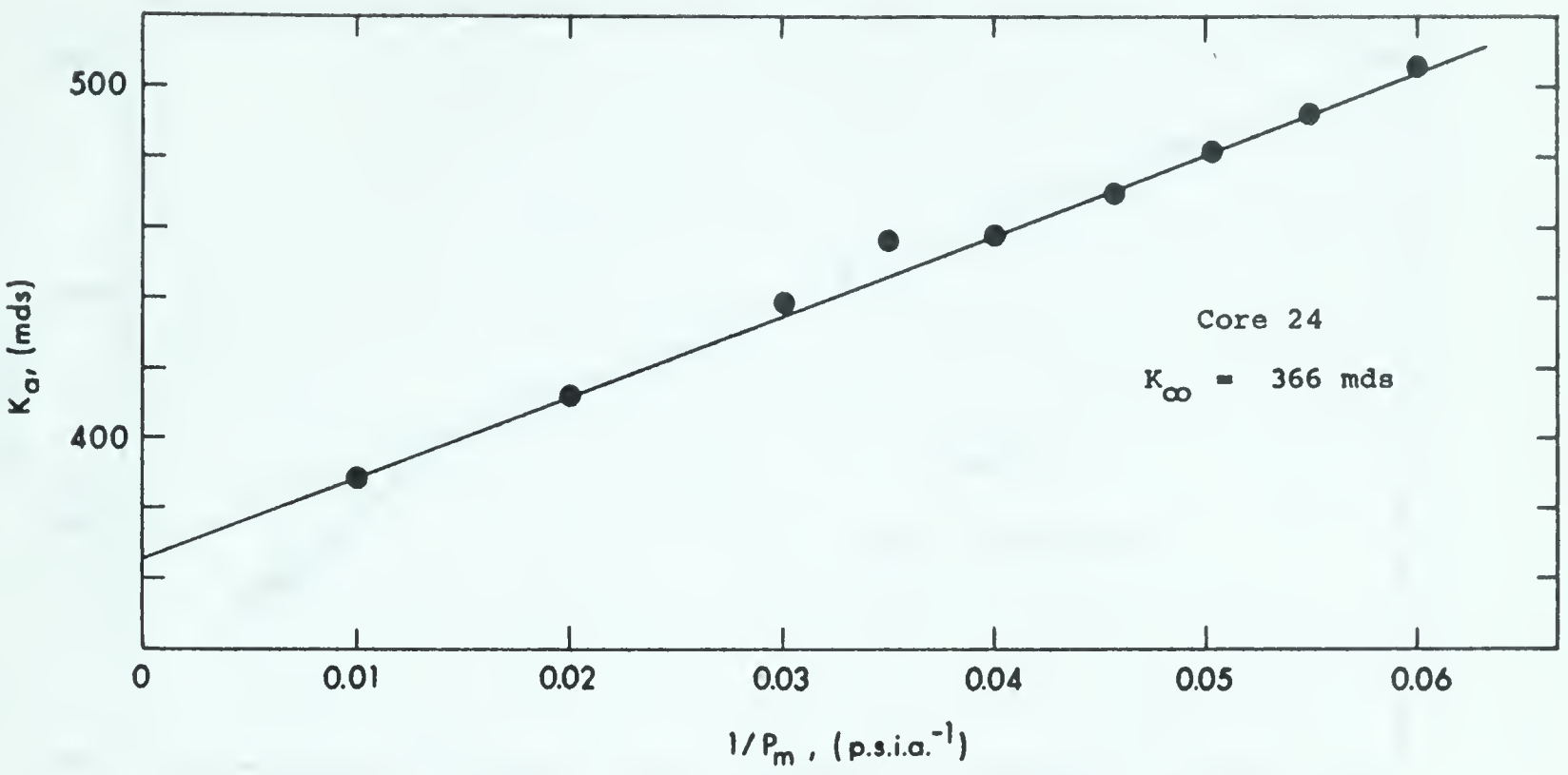

Figure 7-A. Klinkenberg Permeability Plot

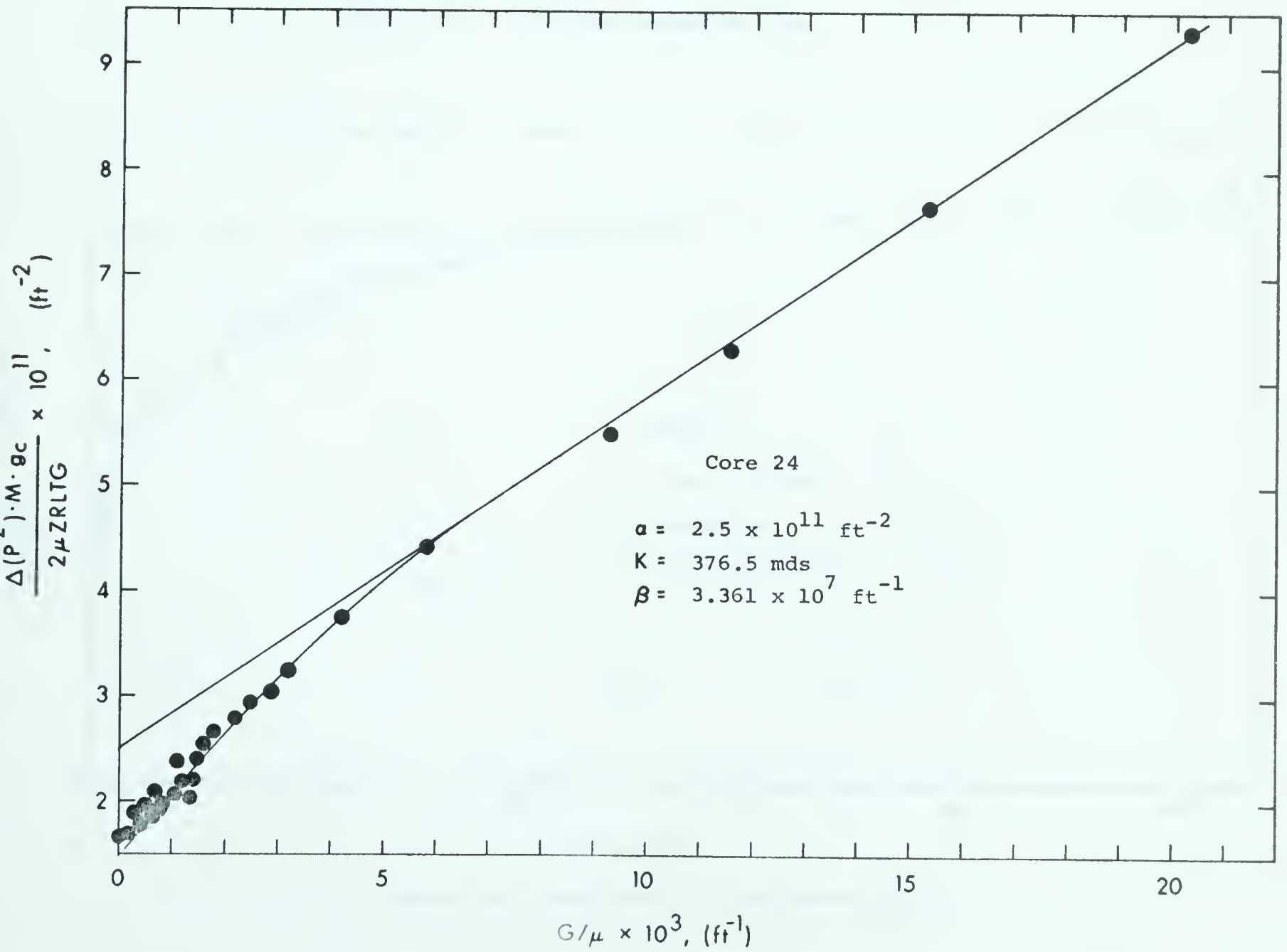

Figure 8-A. Flow Data Plot to Calculate α and β

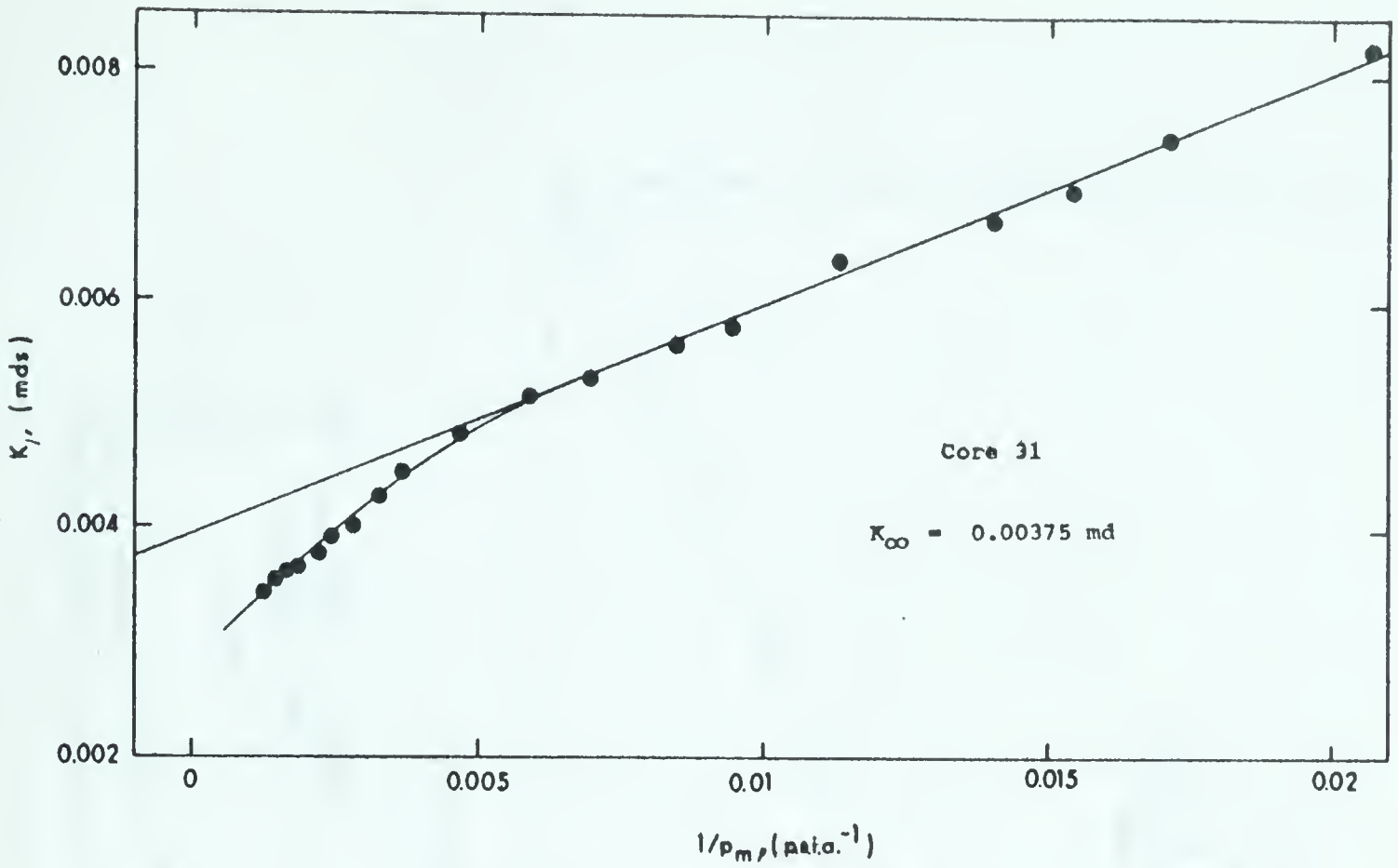

Figure 9-A. Klinkenberg Permeability Plot

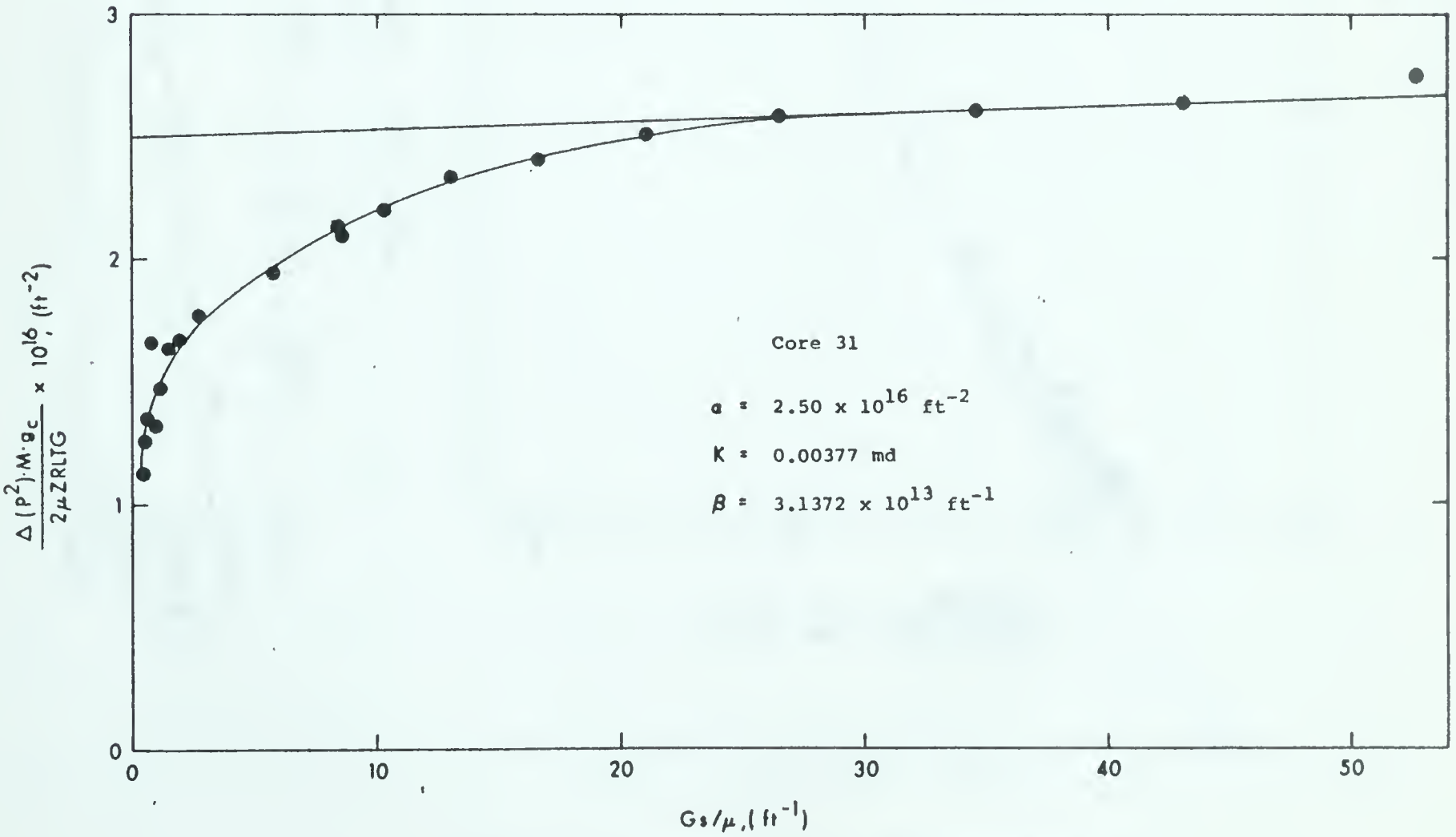

Figure 10-A. Flow Data Plot to Calculate α and β

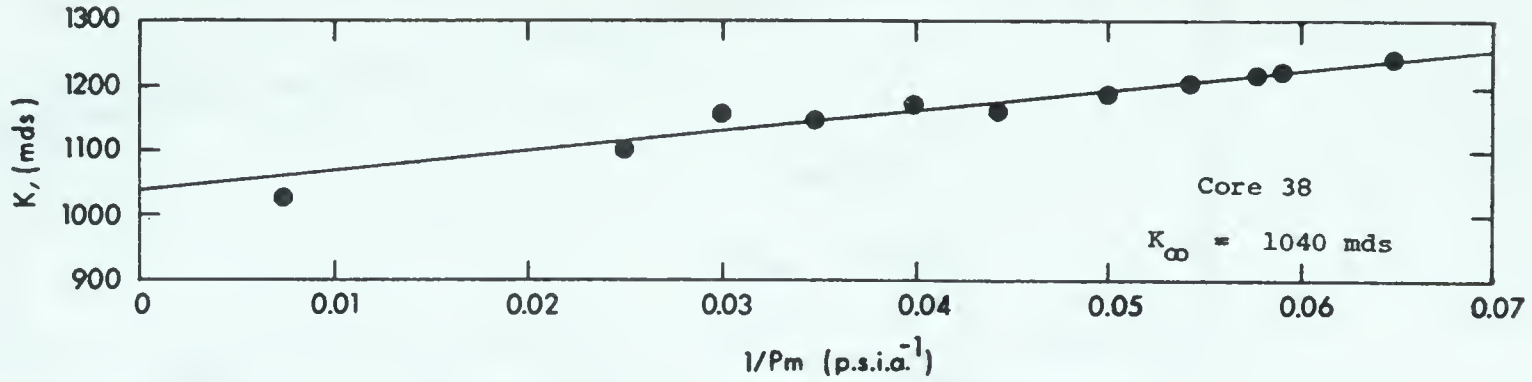

Figure 11-A. Klinkenberg Permeability Plot

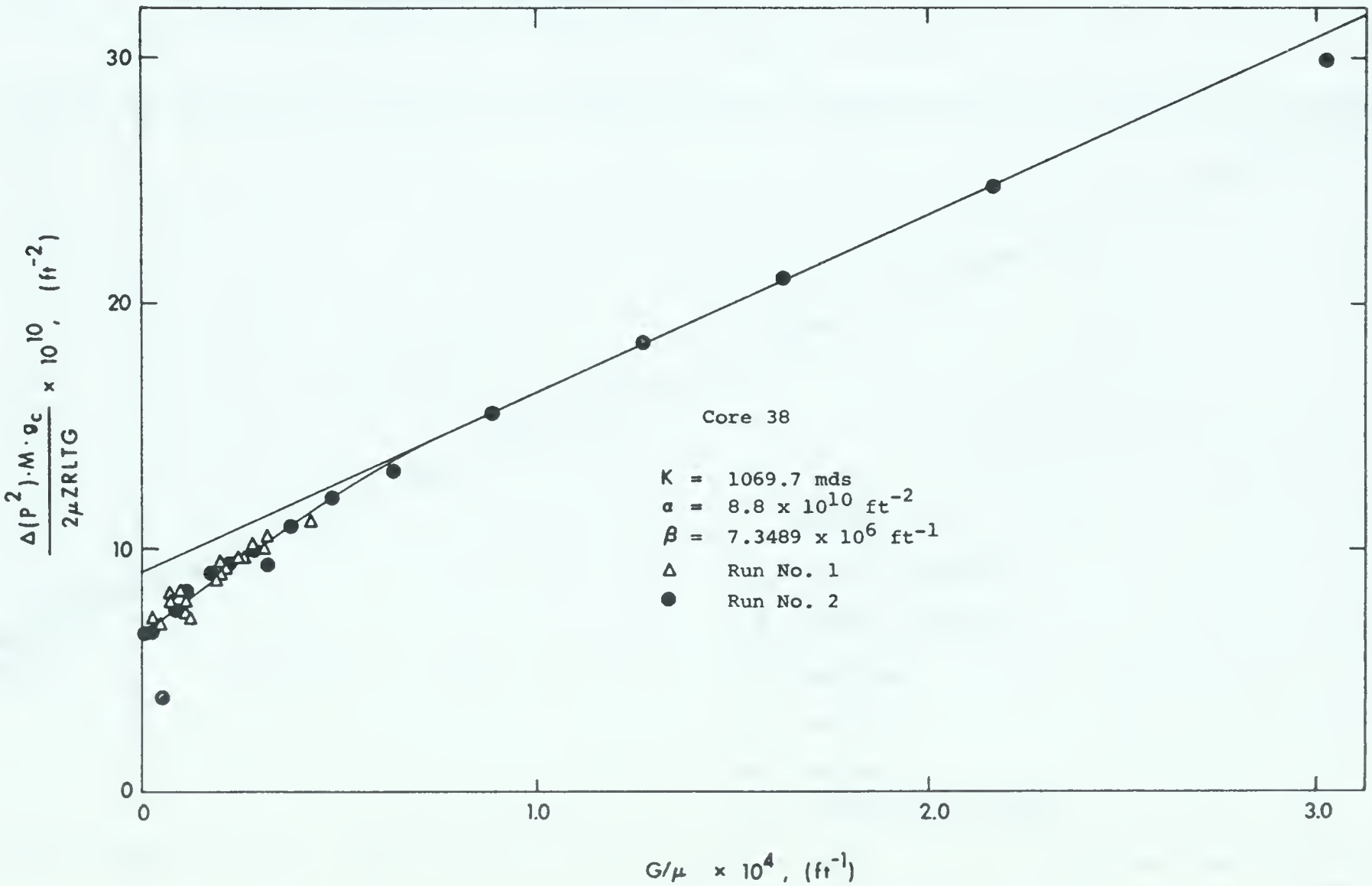

Figure 12-A. Flow Data Plot to Calculate α and β

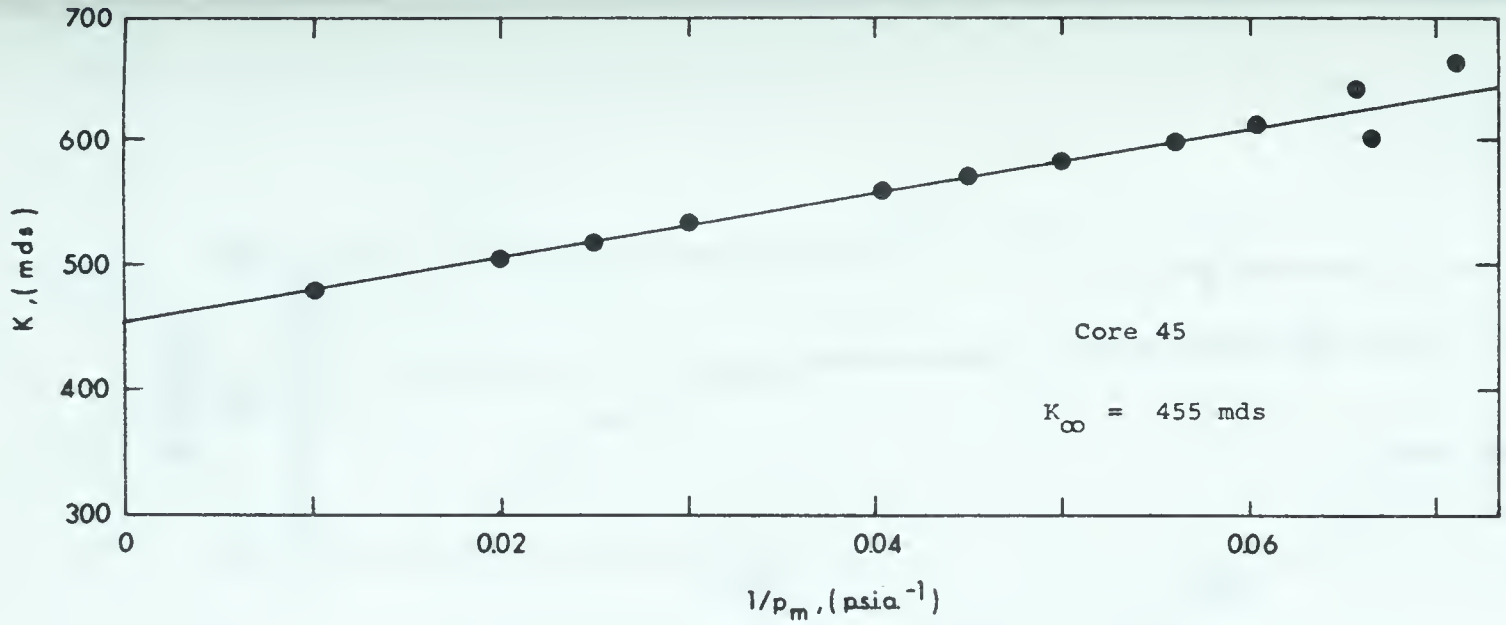

Figure 13-A. Klinkenberg Permeability Plot

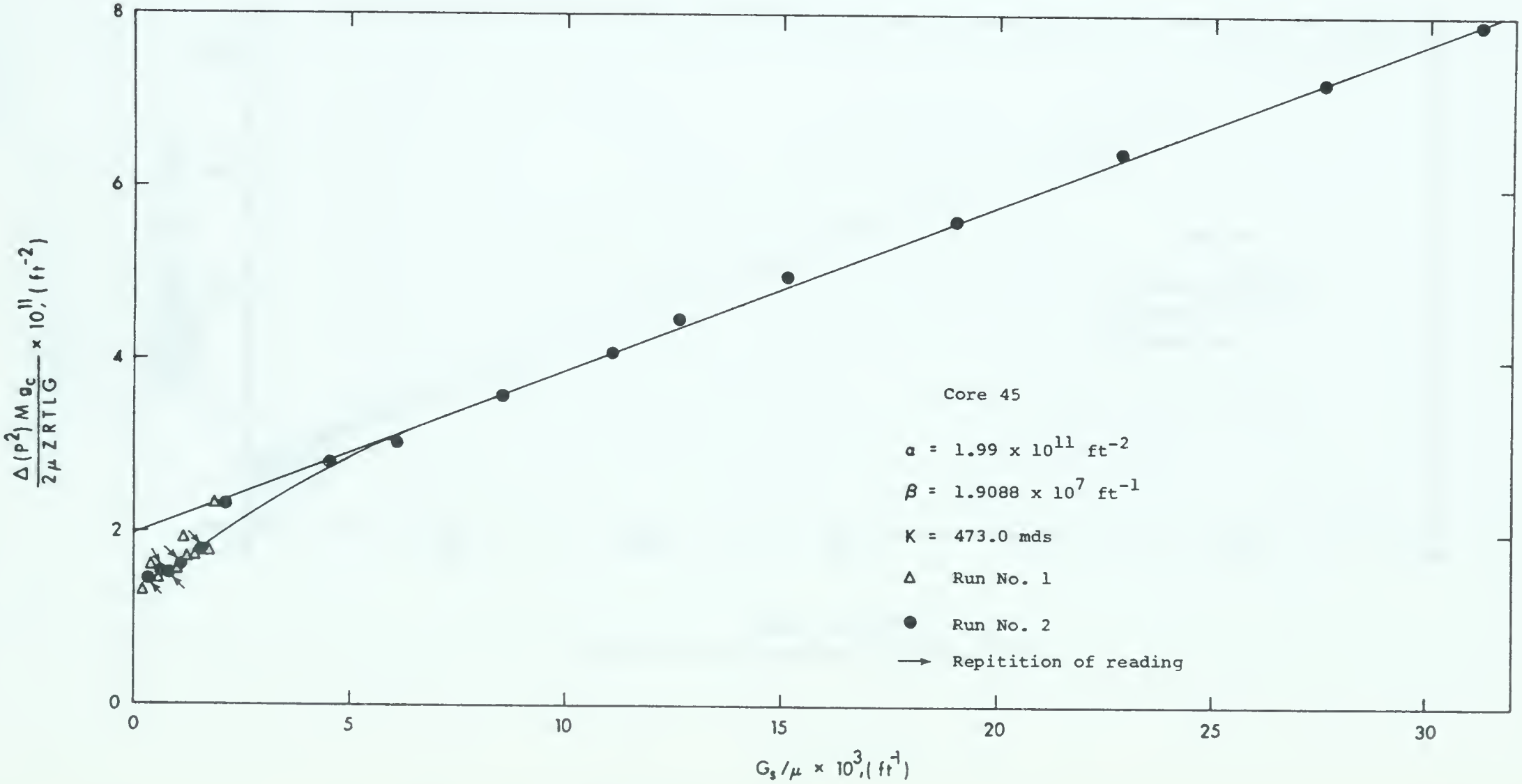

Figure 14-A. Flow Data Plot to Calculate α and β

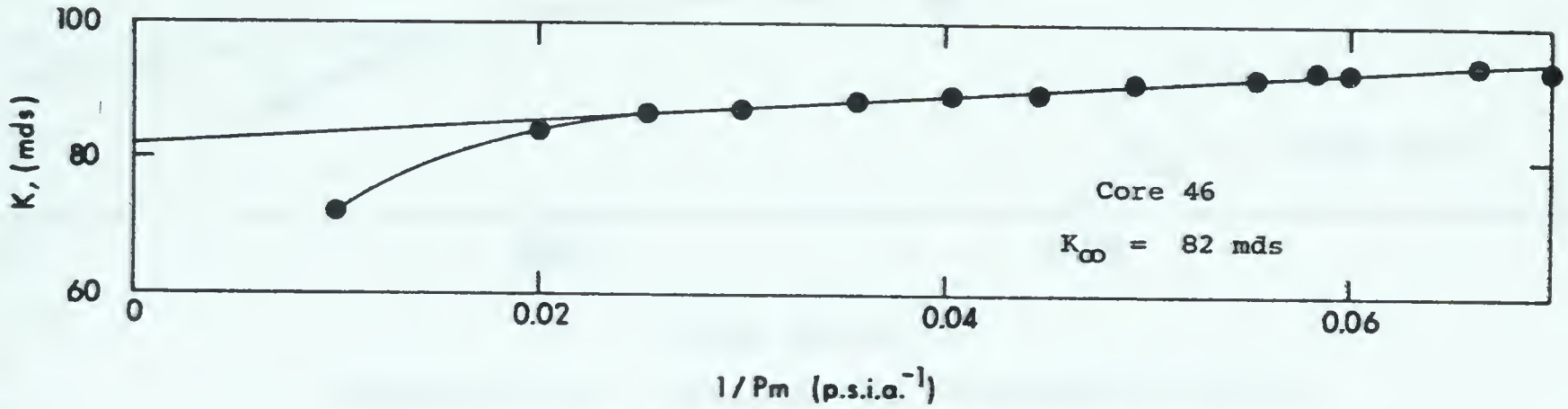

Figure 15-A. Klinkenberg Permeability Plot

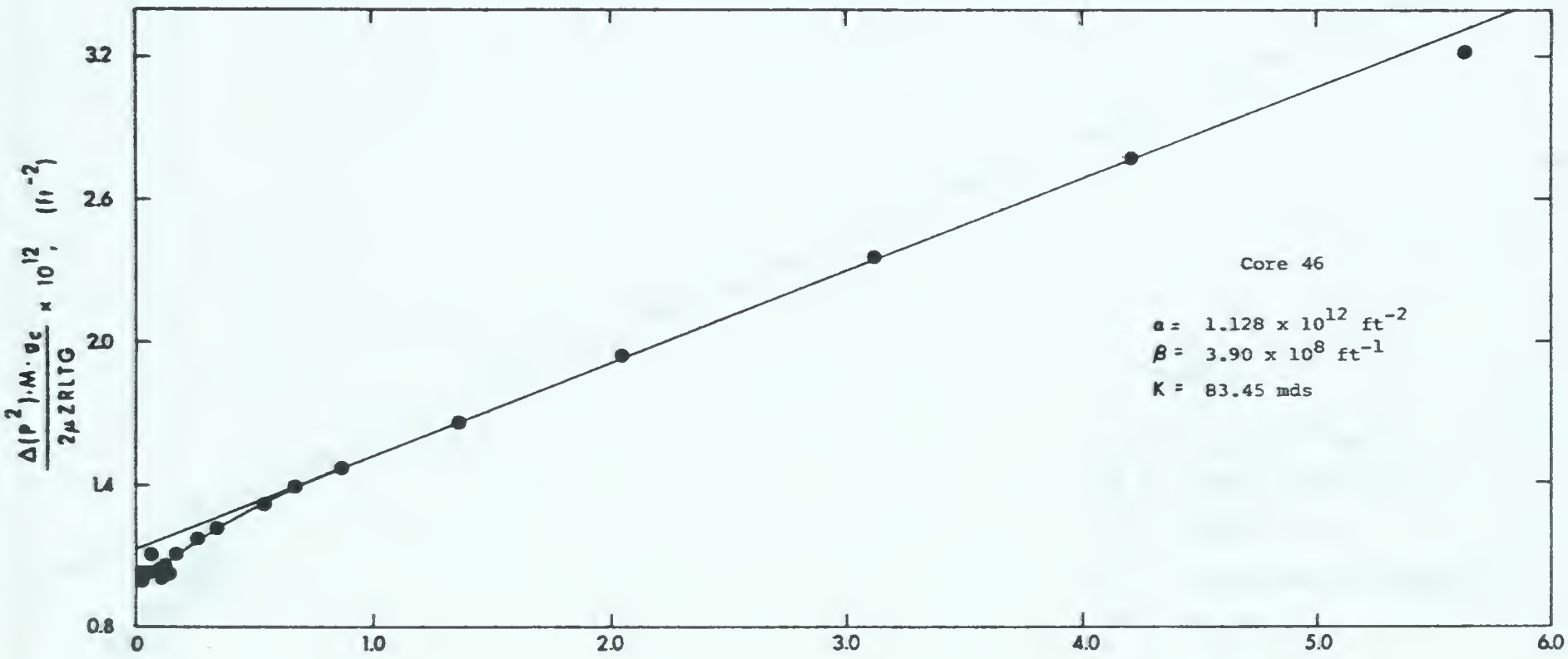

Figure 16-A. Flow Data Plot to Calculate α and β

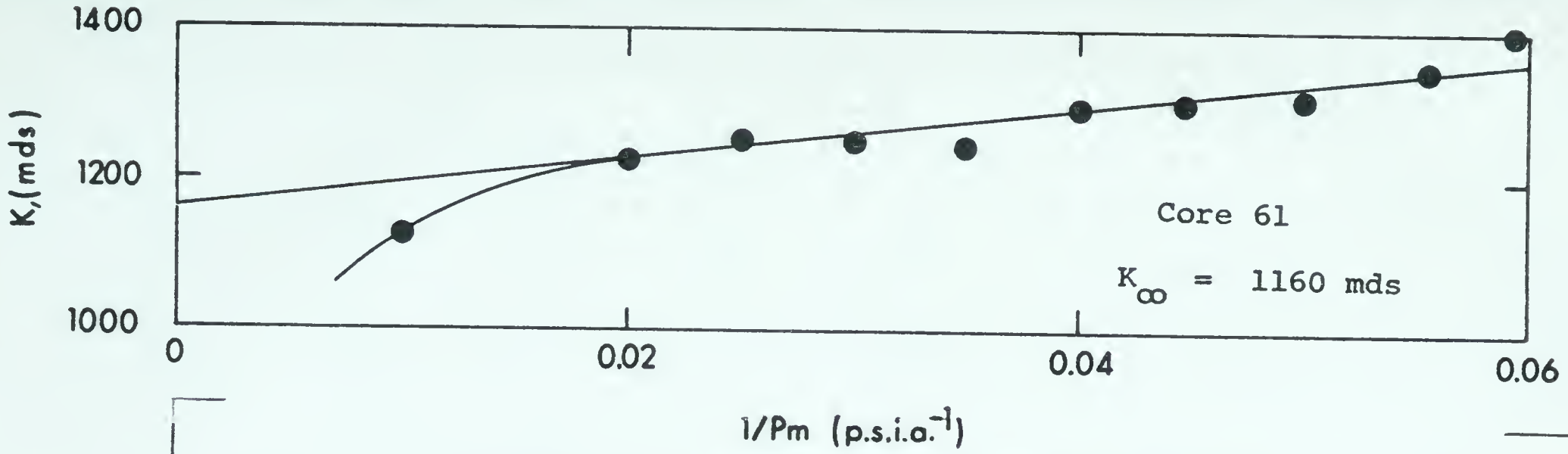

Figure 17-A. Klinkenberg Permeability Plot

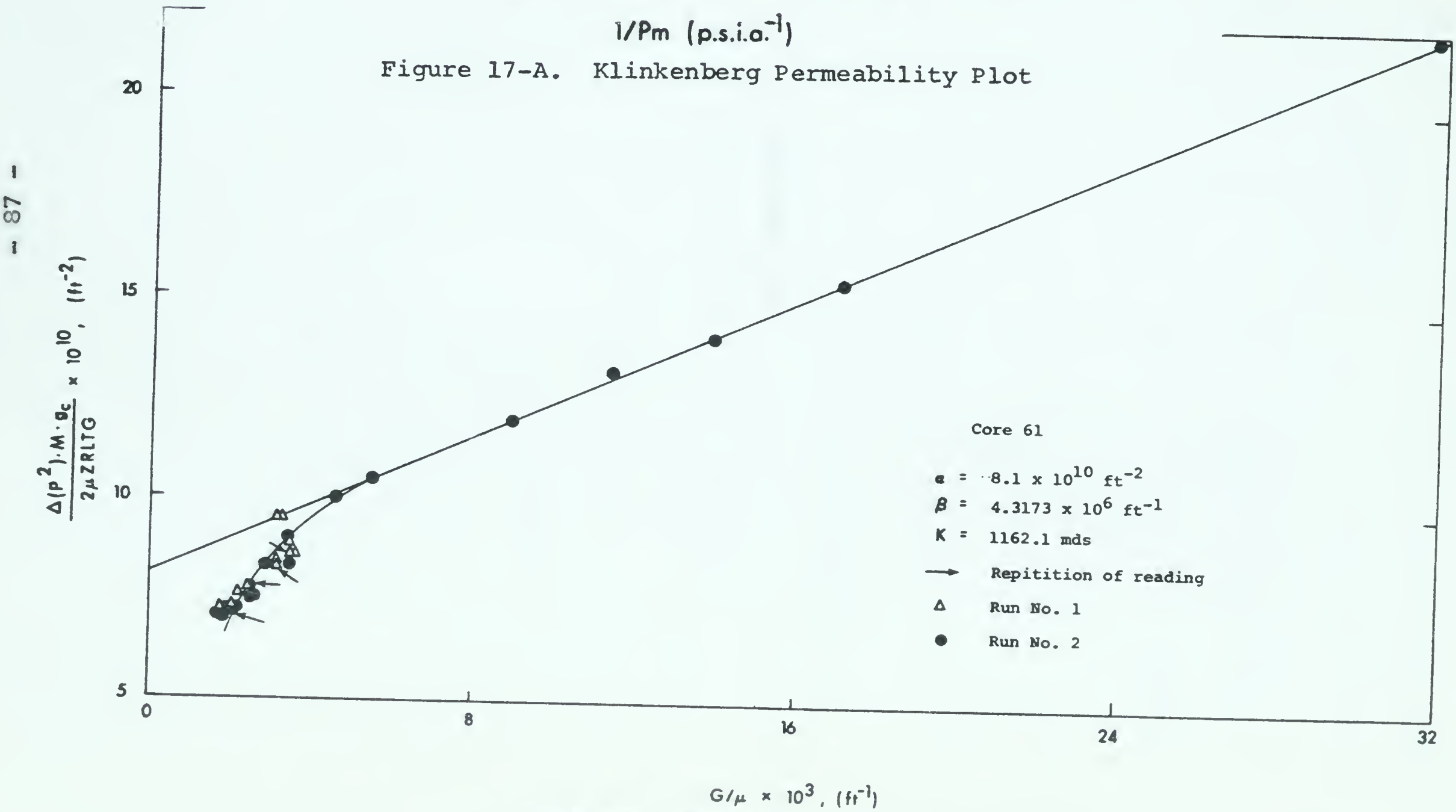

Figure 18-A. Flow Data Plot to Calculate α and β

APPENDIX III

EQUATIONS

$$Q_m = \frac{2\ Q_c\ P_b}{(P_1 + P_2)} \cdot \frac{T_f}{T_b}$$

Q_m = flow rate at mean pressure and flowing temperature

Q_c = flow rate at standard conditions, 14.65 psia and 60°F

P_b = pressure base = 14.65 psia

T_f = average flowing temperature in °R

T_b = temperature base = 60°F

P_1 = upstream pressure

P_2 = downstream pressure

$$K_a = \frac{Q_m}{A} \frac{\mu L}{P_1 - P_2} = 2Q_c \frac{P_b}{(P_1^2 - P_2^2)} \cdot \frac{\mu L}{A} \cdot \frac{T_f}{T_b}$$

K_a = darcies

μ = cp

Q = cc/sec

L = cm

P = atm

A = cm^2

T = °R

$$K_a = 0.25573 \frac{Q_c \, T_f \, \mu \, L}{(\Delta P^2) \, A}$$

K_a = millidarcies

T_f = °R

μ = micropoise

L = in

A = in^2

P = psia

Q_c = SCFH

$$\frac{M \, g_c}{2(ZRT) \, \mu \, L} = 52.0956 \times 10^6 \cdot \frac{1}{Z T_f \mu L} \frac{lb_m}{lb_f^2 \, sec}$$

Z = compressibility

T_f = °R

μ = micropoise

L = in.

$$G = G_S = \frac{Q_c \rho}{A} = .04 \frac{Q_c \rho}{A} \frac{lb_m}{ft^2 \, sec}$$

Q = SCFH

ρ = lb_m/ft^3

A = in^2

$$\frac{\Delta(P^2)}{G} = 20736 \frac{\Delta(P^2)}{G} \frac{lb_f^2 \, sec}{lb_m \, ft^2}$$

P = psia

$$\frac{G}{\mu} = 148.8 \times 10^5 \frac{G}{\mu} \; ft^{-1}$$

G = $\frac{lb_m}{ft^2 \, sec}$

μ = micropoise

$$Q_c = Q \times \text{meter correction factor} \times \frac{P_M}{T_M} \times 35.495$$

Q = CFH

P_M = meter inlet pressure in psia

T_M = meter inlet temperature °R

$$P_M = P_{atm} + P_{\text{meter inlet (psig)}} - \text{partial pressure of water}$$

SAMPLE CALCULATIONS

Klinkenberg Permeability Data

Core No. 53 - Taber sandstone

Area = 0.7775 in^2 Length = 1.5593 in.

Posority = 22.06%

Q = flow rate = 2.7975 CFH

Temperature = 535.5°R

Pressure atmospheric = 69-87 cm Hg = 13.464

Flowing fluid - nitrogen

Average flowing temperature = 538.0 °R

μ (avg. temp. and pressure) = 177.875 micropoise

P_1 = 21.504 psia

P_2 = 13.884 psia

P_{meter} = 13.464 psia

P_{base} = 14.65 psia

T_{base} = 520°R

$\Delta(P^2)$ = 269.66 $(psia)^2$

water differential on the manometer = 0

Calculations

1. $Q_{SCFH} = Q_{(meter)} \times$ meter correction factor $\times \frac{P_{meter}}{T_{meter}} \times \frac{T_{base}}{P_{base}}$

$Q_{SCFH} = Q_c = 2.4715$

2. $K_a = 0.25573 \dfrac{Q_c\ T_f\ \mu\ L}{\Delta\ (P^2)\ A}$

$= 450$ mds

3. $G_s = 0.04 \dfrac{Q_c \rho}{A} = 9.362 \times 10^{-3}$ lb_m/ft^2 sec

4. $\dfrac{G_s}{\mu} = 148.8 \times 10^5 \times \dfrac{G_s}{\mu}$

$= 783.17$ ft^{-1}

5. $\dfrac{\Delta(P^2)}{G_s} = 20736 \dfrac{\Delta(P^2)}{G_s}$

$= 5.9726 \times 10^8$ $lb_f{}^2\text{-sec}/lb_m\text{-ft}^2$

6. $\dfrac{M\ g_c}{2(ZRT)\mu L} = \dfrac{52.0956 \times 10^6}{T_f\ \mu\ Z\ L}$

$= 3.4907 \times 10^2$ $lb_m/ft^2\text{-sec}$

7. $\dfrac{M\ g_c\ \Delta(P^2)}{2(ZRT)\mu LG} = 2.0849 \times 10^{11}$ (ft^{-2})

B29831